JAN 2 1986

NUREG/CR-3900
Vol. 3

COMPLETED 97.

Long-Term Performance of Materials Used for High-Level Waste Packaging

Third Quarterly Report, Year Three
October - December 1984

Compiled by D. Stahl, N. E. Miller

Battelle's Columbus Laboratories

Prepared for
U.S. Nuclear Regulatory
Commission

ORIGINAL

BEST COPY AVAILABLE

NOTICE

This report was prepared as an account of work sponsored by an agency of the United States Government. Neither the United States Government nor any agency thereof, or any of their employees, makes any warranty, expressed or implied, or assumes any legal liability of responsibility for any third party's use, or the results of such use, of any information, apparatus, product or process disclosed in this report, or represents that its use by such third party would not infringe privately owned rights.

NOTICE

Availability of Reference Materials Cited in NRC Publications

Most documents cited in NRC publications will be available from one of the following sources:

1. The NRC Public Document Room, 1717 H Street, N.W.
   Washington, DC 20555
2. The Superintendent of Documents, U.S. Government Printing Office, Post Office Box 37082, Washington, DC 20013-7982
3. The National Technical Information Service, Springfield, VA 22161

Although the listing that follows represents the majority of documents cited in NRC publications, it is not intended to be exhaustive.

Referenced documents available for inspection and copying for a fee from the NRC Public Document Room include NRC correspondence and internal NRC memoranda; NRC Office of Inspection and Enforcement bulletins, circulars, information notices, inspection and investigation notices; Licensee Event Reports; vendor reports and correspondence; Commission papers; and applicant and licensee documents and correspondence.

The following documents in the NUREG series are available for purchase from the NRC/GPO Sales Program: formal NRC staff and contractor reports, NRC-sponsored conference proceedings, and NRC booklets and brochures. Also available are Regulatory Guides, NRC regulations in the *Code of Federal Regulations*, and *Nuclear Regulatory Commission Issuances*.

Documents available from the National Technical Information Service include NUREG series reports and technical reports prepared by other federal agencies and reports prepared by the Atomic Energy Commission, forerunner agency to the Nuclear Regulatory Commission.

Documents available from public and special technical libraries include all open literature items, such as books, journal and periodical articles, and transactions. *Federal Register* notices, federal and state legislation, and congressional reports can usually be obtained from these libraries.

Documents such as theses, dissertations, foreign reports and translations, and non-NRC conference proceedings are available for purchase from the organization sponsoring the publication cited.

Single copies of NRC draft reports are available free, to the extent of supply, upon written request to the Division of Technical Information and Document Control, U.S. Nuclear Regulatory Commission, Washington, DC 20555.

Copies of industry codes and standards used in a substantive manner in the NRC regulatory process are maintained at the NRC Library, 7920 Norfolk Avenue, Bethesda, Maryland, and are available there for reference use by the public. Codes and standards are usually copyrighted and may be purchased from the originating organization or, if they are American National Standards, from the American National Standards Institute, 1430 Broadway, New York, NY 10018.

BEST COPY AVAILABLE

NUREG/CR-3900
Vol. 3

Long-Term Performance of Materials Used for High-Level Waste Packaging

Third Quarterly Report, Year Three
October - December 1984

Manuscript Completed: March 1985
Date Published: May 1985

Compiled by
D. Stahl, N. E. Miller

Battelle's Columbus Laboratories
505 King Avenue
Columbus, OH 43201-2693

Prepared for
Division of Radiation Programs and Earth Sciences
Office of Nuclear Regulatory Research
U.S. Nuclear Regulatory Commission
Washington, D.C. 20555
NRC FIN B6764
Under Contract No. NRC 04-82-015

I

BEST COPY AVAILABLE

BLANK PAGE

ABSTRACT

As part of the Nuclear Regulatory Commission's requirement to assess the Department of Energy's application to construct geologic repositories for storing high-level radioactive waste, Battelle's Columbus Laboratories is investigating the long-term performance of materials used for high-level waste packaging. Experiments for evaluating the glass-dissolution model are under way, and the procedure developed last quarter for dispersing RuO_2 in MCC 76-68 glass has been tested and proved to produce appropriate particle concentrations. Acetic and humic acids have been chosen to test the effect of natural organic acids on waste-glass performance. In the overpack-corrosion effort, potentiodynamic polarization tests indicate that of the 15 chemical species tested, all but perchlorate and hydrogen may affect stress-corrosion cracking behavior of carbon steel; several synergistic effects were also indicated. In slow strain rate studies, specimens tested in 0.0005 M $FeCl_3$ (a much lower chloride concentration than expected in groundwater) exhibited significant cracking over the temperature range 250-315 C. Pits were found to propagate readily, but slowly, in 1018 carbon steel exposed to aerated basalt groundwater at 90 C. The general-corrosion correlation was changed to incorporate a finite rate of film growth. Integral experiments are being prepared to provide information on combined-effects processes that may influence the long-term performance of the waste package.

This report documents investigations performed during the period October-December 1984.

BEST COPY AVAILABLE

CONTRIBUTORS

J. A. Beavers
H. J. Cialone
M. P. Failey
J. H. Holbrook
A. J. Markworth
J. K. McCoy
S. L. Nicolosi
M. R. Pascucci
E. D. Spinosa
N. G. Thompson

BEST COPY AVAILABLE

TABLE OF CONTENTS

	Page
ABSTRACT	iii
1. INTRODUCTION: PROJECT OBJECTIVES AND APPROACH	1-1
1.1 Individual Program Tasks	1-2
1.1.1 Waste Forms	1-2
1.1.2 Container Materials	1-2
1.1.3 Integrated System Performance	1-3
1.2 Overall Program Objectives	1-4
2. WASTE FORMS	2-1
2.1 Glass-Dissolution Model	2-1
2.2 Crystallinity Influences	2-1
2.3 Organic Acid Experiment	2-6
2.4 Water Chemistry and Waste-Form Dissolution Modeling	2-11
2.5 References for Section 2	2-12
3. CONTAINER MATERIALS	3-1
3.1 External Corrosion	3-1
3.1.1 Potentiodynamic Polarization Studies	3-2
3.1.1.1 Experimental Effort	3-2
3.1.1.2 Statistical Methodology	3-5
3.1.1.3 Results	3-7
3.1.2 Slow Strain Rate Studies	3-17
3.1.3 Pit-Propagation Experiments	3-20
3.2 Hydrogen Embrittlement	3-28
3.2.1 Fracture-Toughness Tests	3-29
3.2.2 Results and Discussion	3-29
3.2.3 Future Work	3-32
3.3 Corrosion Correlations	3-32
3.3.1 General Corrosion	3-32
3.3.2 Pitting Corrosion	3-34
3.4 References for Section 3	3-36

BEST COPY AVAILABLE

TABLE OF CONTENTS
(Continued)

	Page
4. INTEGRATED SYSTEM PERFORMANCE.	4-1
4.1 Groundwater-Radiolysis Studies.	4-1
4.1.1 Effects of G-Value Sets on Calculated Concentrations	4-2
4.1.2 Generation of G-Values to Correlate with Benchmark Data	4-4
4.1.3 Conclusions.	4-6
4.2 Integral Experiments.	4-6
4.2.1 Status	4-6
4.2.2 Future Work.	4-7
4.3 References for Section 4.	4-7
5. QUALITY ASSURANCE.	5-1

BEST COPY AVAILABLE

LIST OF FIGURES

		Page
Figure 2.1.	pH of leachant after exposure of sample at MCC-1P conditions	2-3
Figure 2.2.	Percent specimen weight loss after exposure to MCC-1P conditions	2-4
Figure 2.3.	Analyzed concentration of silicon in leachant after sample exposure to MCC-1P conditions	2-5
Figure 2.4.	Photomicrographs of thin sections of RuO_2-doped MCC 76-68.	2-7
Figure 2.5.	Coordinates and levels of central composite design	2-9
Figure 3.1.	Schematic of typical anodic potentiodynamic polarization curves.	3-4
Figure 3.2.	Potentiodynamic polarization curves for 1020 carbon steel in solution 11	3-8
Figure 3.3.	Potentiodynamic polarization curves for 1020 carbon steel in solution 14	3-9
Figure 3.4.	Potentiodynamic polarization curves for 1020 carbon steel in solution 20	3-10
Figure 3.5.	Low-power optical photograph of gauge length of hot-rolled 1020 carbon steel specimen tested in 0.001 M $FeCl_3$ at 315 C at a strain rate of 6×10^{-7}/s	3-19
Figure 3.6.	Optical photographs of metallographic section of hot-rolled 1020 carbon steel specimen tested in 0.001 M $FeCl_2$ at 315 C at a strain rate of 6×10^{-8}/s	3-21
Figure 3.7.	Optical photograph of metallographic section of hot-rolled 1020 carbon steel specimen tested in 0.0005 M $FeCl_3$ at 315 C at a strain rate of 1×10^{-7}/s	3-22
Figure 3.8.	Effect of temperature on crack velocity and crack depth for hot-rolled 1020 carbon steel tested in 0.0005 M $FeCl_3$ at a strain rate of 1×10^{-7}/s.	3-23

BEST COPY AVAILABLE

LIST OF FIGURES
(Continued)

		Page
Figure 3.9.	Optical photograph of metallographic section of hot-rolled 1020 carbon steel specimen tested in 0.0005 M $FeCl_3$ at 275 C at a strain rate of 1 x 10^{-7}/s.	3-24
Figure 3.10.	Optical photograph of metallographic section of hot-rolled 1020 carbon steel specimen tested in 0.0005 M $FeCl_3$ at 250 C at a strain rate of 1 x 10^{-7}/s.	3-25
Figure 3.11.	Schematic of pit propagation monitor	3-26
Figure 3.12.	J-resistance curves for iron specimens	3-30

BEST COPY AVAILABLE

LIST OF TABLES

		Page
Table 2.1.	Partial results of glass corrosion model experiments	2-2
Table 2.2.	Results of crystallinity experiment	2-8
Table 2.3.	Organic acid test conditions.	2-11
Table 3.1.	High and low concentrations of species selected for evaluation in the electrochemical experiments	3-5
Table 3.2.	Partial factorial design to be used for the potentiodynamic polarization screening tests.	3-6
Table 3.3.	Experimentally-measured polarization parameters for the 33 test solutions defined in Table 3.2.	3-11
Table 3.4.	Results of statistical analysis indicating the effect of each chemical species on the polarization parameters measured by potentiodynamic polarization.	3-13
Table 3.5.	Results of statistical analysis indicating the effect of groups of interactions on the polarization parameters measured by potentiodynamic polarization.	3-14
Table 3.6.	Summary of results of statistical analysis for the main effects of the chemical species based on a 90 percent or greater probability of significance.	3-15
Table 3.7.	Main effects and interactions selected from screening tests to be examined in the main test matrix	3-16
Table 3.8.	Summary of results of slow strain rate experiments performed on hot-rolled 1020 carbon steel in $FeCl_3$ solutions.	3-18
Table 4.1.	G-values used by various investigators for related systems	4-3
Table 4.2.	Calculated concentrations, pH, and K_W for a water-radiolysis simulation using various sets of G-values	4-3

BEST COPY AVAILABLE

LIST OF TABLES
(Continued)

		Page
Table 4.3.	G-value sets generated to improve agreement with benchmark data	4-5
Table 4.4.	Calculated concentrations, pH, and K_w for a water-radiolysis simulation using G-values chosen to improve agreement with benchmark data . .	4-5
Table 5.1.	Status of NRC waste packaging program QA procedures.	5-2

BEST COPY AVAILABLE

1. INTRODUCTION: PROJECT OBJECTIVES AND APPROACH

The Waste Policy Act of 1982 delegates to the Department of Energy (DOE) the authority for siting, construction, and operation of deep-mined geologic repositories for the disposal of high-level waste and spent fuel. The Nuclear Regulatory Commission (NRC) has the responsibility to regulate the activities of DOE to assure that the health and safety of the repository workers and of the public are adequately protected. Prior to construction, the DOE will submit a license application to the NRC describing in detail the proposed repository. The DOE has been directed to take a multiple barrier approach to the isolation of radioactive wastes with the waste package, the engineered facility, and the natural geohydrologic features of the site being the major barriers. Since NRC's compliance assessment requires the technical capability to understand relevant phenomena and processes relating to the long-term performance of the multiple barriers, the NRC's Office of Nuclear Regulatory Research (RES) has established this waste-package performance program at Battelle's Columbus Laboratories to provide that part of the input to the assessment. As an important aid to this understanding, Battelle is evaluating total system performance which will integrate separate effects and improve the understanding of the long-term performance of waste-package materials. This will also assist in identifying and evaluating research needs.

It is generally accepted that after repository closure the dominant mechanism to cause the release of radionuclides from the repository is groundwater transport. The generally accepted approach to minimizing the release is to provide a number of different barriers to the dissolution and transport of radionuclides by the groundwater. For a deep-mined repository, the geohydrologic features of the earth itself are expected to be a major barrier to the release of radionuclides. The repository site will be selected so that radionuclides will be isolated for very long times. In addition, engineered features of the repository will act as a barrier to the release of radionuclides. The repository will be constructed so as to minimize disturbing the adjacent rock and to accommodate the thermomechanical effects of the emplaced wastes with a minimum of degradation to its geohydrologic properties. Upon closure, the underground openings and shafts to the surface will be backfilled and sealed to minimize groundwater flow paths.

The waste package--which is the center of this study--will be constructed to provide essentially complete containment of the radionuclides through the period of time in which the repository is heated significantly by decaying fission products. After the container is eventually breached by some process, the waste form must remain sufficiently resistant to groundwater attack to provide high retention of the radionuclides and, together with the repository, to control the release of radionuclides for thousands of years. The objective of our research is to provide an improved understanding of the long-term performance of the materials used for the high-level waste package. More specifically, we are identifying those processes that tend to degrade the performance

BEST COPY AVAILABLE

of the waste-package materials, performing experiments to produce data where data are otherwise lacking on material performance, and analytically modeling the processes to utilize the data to better understand how the processes will affect the material's future performance. In addition, we are identifying areas of work that should be performed by DOE to provide missing data which are beyond the resources of the NRC.

1.1 Individual Program Tasks

The program is being conducted in three parallel efforts: waste-form studies, container studies, and integrated system performance studies. A more detailed summary of achievements can be found in the second annual report for this program (NUREG/CR-3427, Volume 4, June 1984, Section 1).

1.1.1 Waste Forms

The waste-form studies are aimed at first describing and modeling those mechanisms that will alter or "age" the waste form during the containment period, and second, identifying and describing those processes that will influence waste-form dissolution after it is exposed to groundwater. The waste-form studies have been largely centered on borosilicate glasses for both defense and commercial high-level wastes; some effort has also been directed toward evaluating spent fuel as a waste form.

In borosilicate glasses, the glass-forming agents can be expected to be tailored to optimize the waste-form properties for each type of high-level waste. After the waste forms are produced, particularly during the very long period of time after disposal while sealed in their containers, they will experience processes that will cause changes. One detrimental effect is devitrification of the glass, which can lead both to new phases with increased solubility and to cracking of the glass (which is detrimental because it allows a greater surface area of the glass to be contacted by the groundwater). A model has been developed to predict the degree of devitrification that will occur from subsequent reheating in the repository after disposal. Another detrimental effect is cracking, which could be induced by the effects of radiation on glass. A study of the radiation effects on glass has revealed no new approach to evaluating this phenomenon experimentally, so we are largely dependent on the existing literature which indicates that radiation produces only a small effect on glass performance.

1.1.2 Container Materials

The container studies focus on processes that can degrade the metallic waste-package container. The objective is to collect data on the parameters that influence the degradation processes, to identify the controlling parameters, and ultimately to model the degradation processes that determine the long-term performance of the container. The material under study is cast low-carbon steel for use in a basalt repository, which is the material currently favored by DOE.

BEST COPY AVAILABLE

The dominant degradation processes that affect the outside of the container are general corrosion, stress-corrosion cracking, pitting, crevice corrosion, hydrogen attack, and mechanical stress. These processes may occur individually or in combination. The parameters that affect these processes include chemical composition and physical state of the steel, groundwater composition and flow rate, temperature, radiation intensity, availability of air, lithostatic forces, redox state, alkalinity/acidity, and availability of hydrogen. These can produce general corrosion, in which the rate of general corrosion will determine the necessary wall thickness, or localized corrosion (such as pitting or crevice corrosion), in which the rate of the localized attack and the container life must be used to establish the wall thickness.

If the steel is susceptible to cracking in the expected environment, the rate of cracking is so rapid relative to required container life that the corrosion-allowance approach cannot be used to achieve acceptable performance. What is important is the susceptibility of the metal to crack initiation. Cracking may result from stress-corrosion cracking or from reduction in fracture toughness from hydrogen attack. Both of these processes are under investigation.

In addition, a comprehensive mathematical model is under development for use in understanding the corrosion processes associated with the waste-container materials in a repository environment. The model computes the fluxes of corrosive species to the container surface, taking into account the fact that certain corrosive species may be generated by radiolysis, and also accounts for diffusion and convective flow to transport the species. The modeling effort is also being applied to pitting attack and considers three different aspects of the overall pitting process: pit-initiation kinetics, pit-growth kinetics, and the evolution of the pit-depth distribution. These analytical efforts are well integrated with the experimental efforts and are being directed to providing an understanding of the long-term performance of the container materials, with emphasis on those processes that can lead to poor performance.

1.1.3 Integrated System Performance

The waste-package system studies interact with the waste-form studies and the container-material studies to provide an improved understanding of the performance of the total waste-package system. The current emphasis is on providing information for a better understanding of the processes involved in waste-package system degradation. One aspect of the total system under study is the production of radiolysis products in the groundwater by gamma radiation from the waste. This is of major importance in modeling the corrosion of the container and in planning experiments to determine the effects of radiolysis. Our radiolysis model is based on existing codes and sets of chemical reactions combined to provide the best description of experimental data found in the literature. The output of the radiolysis model calculations provides input to the water-chemistry model, which is a fundamental part of the glass-dissolution model and the general-corrosion model.

BEST COPY AVAILABLE

The water-chemistry model which we initially developed for our use with our glass-dissolution and corrosion models has intentionally been kept simple. Simplifying assumptions were made and only a limited set of chemical species was used. This set included the basic water species, the species which dominate most natural groundwaters, and certain species which are assumed to result from the corrosion of iron-based metallic containers and from the dissolution of borosilicate glass. Additional species are being incorporated as the model matures. Inputs to the model include temperature, oxidation potential, volume of water, and amounts of each of the elements in solution (including those species from the radiolysis code). The water-chemistry model calculates the concentration and activity of each of the water species.

1.2 Overall Program Objectives

In all the program tasks, the ultimate objective is to develop a base of information to assist the NRC in evaluating the performance of the waste package proposed in DOE's license application. A near-term objective is to provide information to allow the NRC to prepare position papers on the information required of DOE for evaluation of DOE's proposed waste package. Of significance here is identifying sensitive parameters affecting the performance of materials and identifying data requirements.

To achieve the above objectives, the waste-form task is providing information to give a better understanding of the release of radionuclides from the waste form, beginning at the time it is first contacted by groundwater through the 10,000-year period defined in the draft EPA Standard. This includes an understanding of the probable physico-chemical condition of the waste form when it is contacted by groundwater, as well as the parameters of waste-form composition and environmental conditions which will cause changes from its state at the time of disposal. In addition, we are producing experimental data on the parameters that affect dissolution of the waste form, including composition of the groundwater and environmental conditions. The waste-form dissolution process is also being mathematically modeled to allow analysis of the performance of the waste form under specific input conditions.

The information on the performance of the container materials relates to the required containment period of up to 300 to 1000 years. The container performance is expected to be most affected by corrosion and hydrogen-attack processes. We are providing information on the parameters of container-material composition, groundwater composition, and environmental conditions that are most significant in these processes. Our studies of cast low-carbon steel in a basalt environment (the container material currently favored by DOE) focus on the susceptibility of the metal to stress-corrosion cracking under repository conditions, because steel is known to fail by this process in some environments. We are studying the chemical species and environmental conditions that cause cracking to determine whether this mode of failure is expected under credible repository conditions. Our experimental studies on

BEST COPY AVAILABLE

general and localized corrosion, together with our comprehensive general-corrosion model, will assist in evaluating the corrosion-allowance approach for the use of steel as a long-life container.

Modeling efforts in the integrated system performance task are contributing significant information to studies of general corrosion and glass dissolution. These studies require knowledge of the amount and kind of chemical species that may be produced by radiolysis of the groundwater near the waste package as a result of gamma radiation from the enclosed waste. To obtain this information, energy deposition and radiolysis codes are used. The ANISN code* is used to calculate the gamma fluxes and energy-deposition rates in and near the waste package over the time after disposal; these have been calculated for commercial high-level waste and for spent-fuel waste forms. The gamma fluxes and energy-deposition rates as a function of time are then used in the water-radiolysis model to calculate the amount and kind of radiolysis products in the groundwater near the waste package. To determine how these radiolysis products may affect the performance of the canister and waste form, it is necessary to determine their chemical activities. These are calculated by the water-chemistry model. The output from the water-chemistry model is the concentration and activity of each chemical species in the groundwater near the waste package. This information is used not only as input to the general-corrosion and glass-dissolution models, but also as a point of reference in directing the experimental efforts in corrosion and dissolution.

---

*W. W. Engle, Jr., "A User's Manual for ANISN, A One-Dimensional Discrete Ordinates Transport Code with Anisotropic Scattering", K-1693, Oak Ridge Gaseous Diffusion Plant, Oak Ridge, TN (March 1967).

BEST COPY AVAILABLE

2. WASTE FORMS

Much of the data needed for verifying the dissolution model was obtained during this reporting period. The dispersion of RuO_2 for the crystallinity experiment was confirmed, and the previously defined experimental matrix was completed. An experimental plan to evaluate possible enhancement of glass corrosion by organic acids found in repositories was devised during this reporting period.

2.1 Glass-Dissolution Model

In an experiment for evaluating a the glass-dissolution model, specimens of MCC 76-68 glass, crystalline quartz (α-quartz), and amorphous silica (a-SiO_2) were exposed to reagent-grade water under MCC-1P conditions. The exposure time varied between 1 and 70 days. Because it had been determined that excessive contact between the glass and the water was undesirable,[2.1] these specimens were in contact with the water only at the experimental temperature for the specified experimental time. After treatment, the glass specimens were removed and weighed. The pH of the leachant was measured, and the leachant was treated with high-purity $NaCO_3$ to ensure that all silicon was dissolved. The concentration of monomeric silica in this solution was determined by an ammonium molybdate colorimetric procedure. The results of the analyses are presented in Table 2.1 and Figures 2.1-2.3. These represent all the data for MCC 76-68 glass and part of the data for α-quartz and a-SiO_2. Those data yet to be measured are marked in Table 2.1.

As can be seen in Figure 2.1, the pH change is much greater for MCC 76-68 than for either of the silica references. The pH for MCC 76-68 seems to tend to an equilibrium value of approximately 8.8, while the pH of the reference specimens tends toward an equilibrium value of around 5.6. The data on weight loss and silicon concentration, shown in Figures 2.2 and 2.3, respectively, are consistent with these pH data and with each other. However, neither of these latter graphs show the peak predicted by the proposed model. The steep slope in these curves implies that the MCC 76-68 glass is still a long way from equilibrium and that longer treatment times will be required to prove or disprove the proposed model.

This experiment will continue for the rest of the program year. The data missing from Table 2.1 will be obtained in the next quarter, and longer exposures will be started. Additional specimens will be withdrawn at two-week intervals starting on the 84th day of the exposure.

2.2 Crystallinity Influences

The objective of this experiment is develop in MCC 76-68 glass two mean crystal sizes, each at two different volume fractions, so that the influence of these parameters on waste-form corrosion can be assessed. The needed crystallinity is to be developed by heat-treating MCC 76-68

BEST COPY AVAILABLE

Table 2.1 Partial results of glass corrosion model experiment.

Exposure, Days	MCC 76-68			α-quartz			a-SiO_2			Blank	
	pH(a)	%ΔW(b)	[Si](c)	pH(a)	%ΔW(b)	[Si](c)	pH(a)	%ΔW(b)	[Si](c)	pH(a)	[Si](c)
1	8.3	0.0172	9.19	--	--	--	--	--	--	--	--
3	8.5	0.572	18.77	--	--	--	--	--	--	--	--
5	8.7	0.0654	22.41	--	--	--	--	--	--	--	--
8	8.7	0.1044	33.04	(d)	(d)	(d)	(d)	(d)	(d)	(d)	(d)
11	8.8	0.1217	38.90	--	--	--	--	--	--	--	--
14	8.9	0.1128	41.14	(d)	(d)	(d)	(d)	(d)	(d)	(d)	(d)
21	9.0	0.1392	46.33	--	--	--	--	--	--	--	--
28	8.9	0.2833	60.50	(d)	(d)	(d)	(d)	(d)	(d)	(d)	(d)
35	8.975	0.2550	40.74	--	--	--	--	--	--	--	--
42	8.775	0.2319	78.78	5.875	-0.0068	0.89	5.115	-0.0046	1.33	5.425	0.075
56	8.965	0.3174	85.92	5.605	-0.0036	(d)	5.725	0.0000	(d)	5.535	(d)
70	9.067	0.5183	(d)	5.960	0.0000	(d)	5.840	0.0502	(d)	5.521	(d)

(a) Final pH. Assumed initial value for reagent grade water is 5.

(b) Percent weight change = $\frac{\text{initial - final}}{\text{initial}} \times 100.$

(c) Concentration of silicon in solution.

(d) Data unavailable at this time.

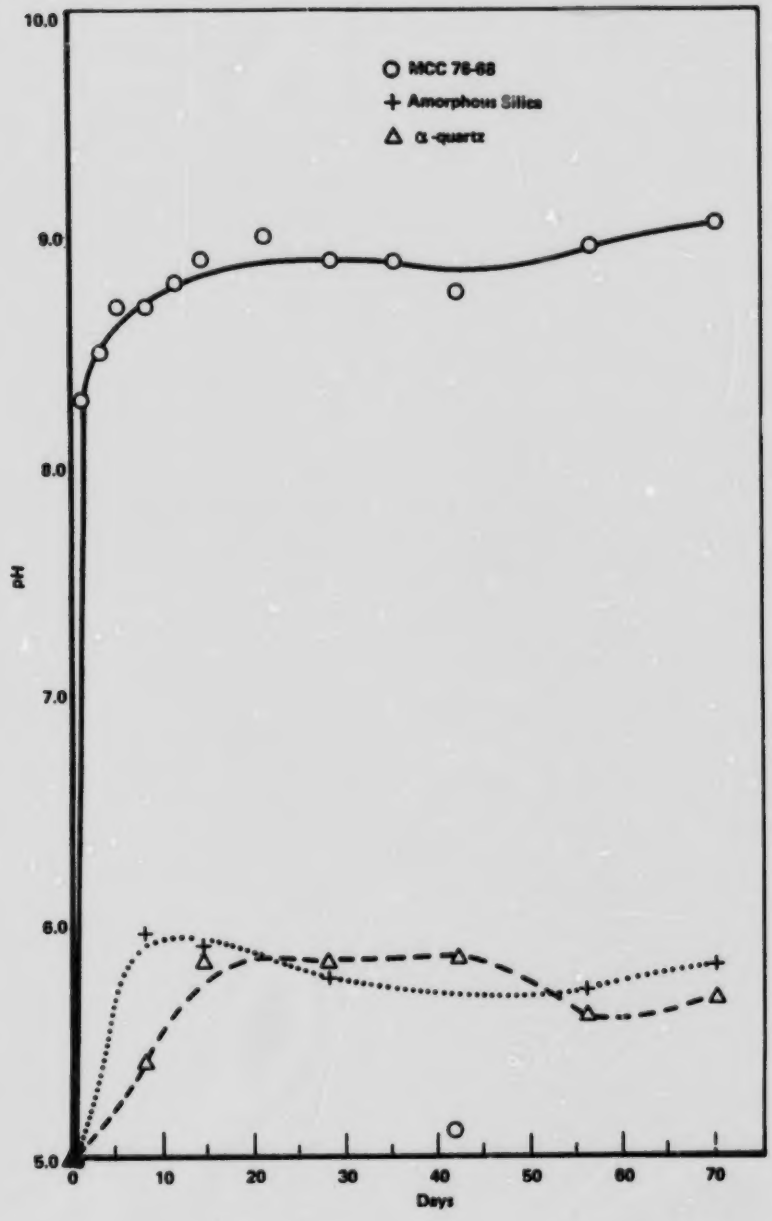

Figure 2.1. pH of leachant after exposure of sample at MCC-1P conditions.

BEST COPY AVAILABLE

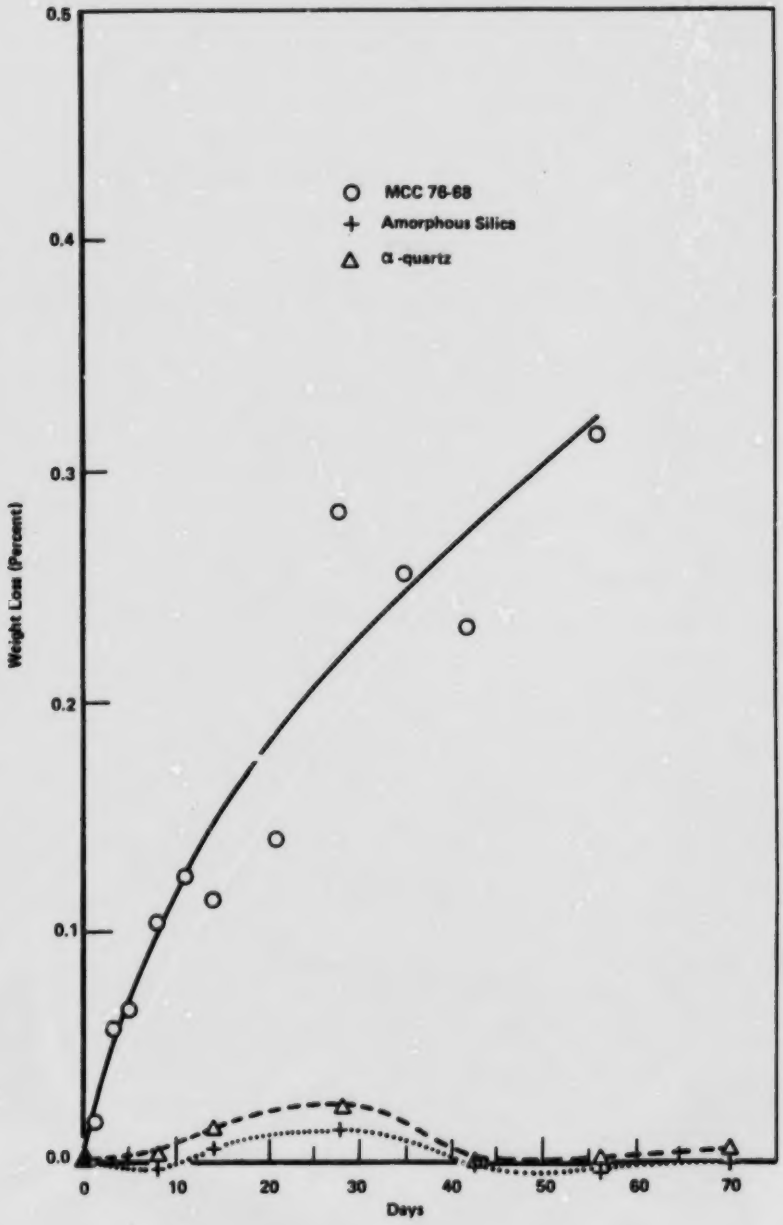

Figure 2.2. Percent specimen weight loss after exposure to MCC-1P conditions.

BEST COPY AVAILABLE

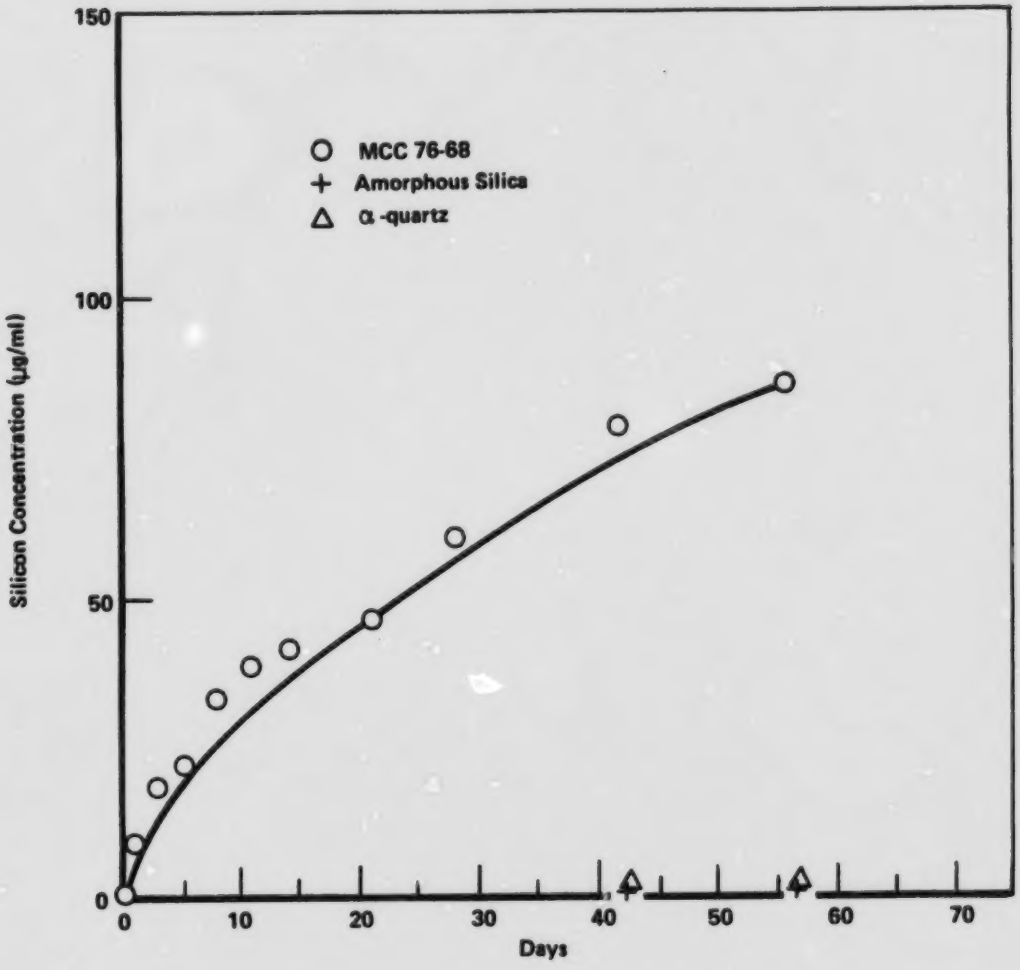

Figure 2.3. Analyzed concentration of silicon in leachant after sample exposure to MCC-1P conditions.

BEST COPY AVAILABLE

glass at several different times, temperatures, and heterogeneous nucleating conditions[2.2]. The nucleant, RuO_2, is a naturally occuring insoluble in the MCC 76-68 melt and a component of the waste streams for which that glass composition has been developed.

Specimens doped at the appropriate level of RuO_2 were prepared by wet dispersion techniques[2.2]. After melting at 1150 C, the glasses were cast into bars and annealed at 450 C. Petrographic thin sections were prepared from two bars with concentrations of nucleating particles of 10^6 and 10^9 per cc. For reference, a sample of undoped MCC 76-68 was similarly prepared. Photographs of these thin sections in transmitted light at 400X are presented in Figure 2.4.

The doped specimens clearly show a concentration of black particles. Since the only difference between these specimens and the undoped reference is the addition of RuO_2, those black particles must be dispersed RuO_2. The micrographs reveal that although some agglomerates remain, the RuO_2 particles, for the most part, are uniformly dispersed. The features that appear to be "bubbles" are interference patterns produced by light scattering from the closely packed RuO_2 particles. Therefore, the doping procedure described in the last report[2.2] does produce the needed particle concentrations of RuO_2.

Small samples were cut from each of the bars and were treated at the time and temperature conditions listed in Table 2.2. Coordinates shown in this table refer to the position of the indicated variables in the overall experimental design (shown in Figure 2.5). A reference sample of undoped MCC 76-68 was included at each indicated time. Observations of their condition are also shown in Table 2.2.

The comments in Table 2.2 represent inferences about crystallinity that could be drawn from visual inspection of the various specimens. Surface crystallinity is easily recognized, but bulk crystallinity must be inferred by changes in contrast between the treated and reference specimens. The true bulk crystalline condition will be determined by microscopic examination. The data in Table 2.1 are presented to indicate the changes induced by the tested variables.

2.3 Organic Acid Experiment

The objective of this experiment is to identify factors that, if operative in a repository environment, may accelerate glass leaching rates. Such factors may include components of the physicochemical composition of the groundwater in contact with the waste package (such as pH, Eh, and the presence of complexing ions such as F^-, Cl^-, and organic acids), as well as processes that may affect glass integrity, such as devitrification. For third-year and early fourth-year testing we have chosen to concentrate on the effects of natural organic acids, which are common

BEST COPY AVAILABLE

400X

a. Undoped

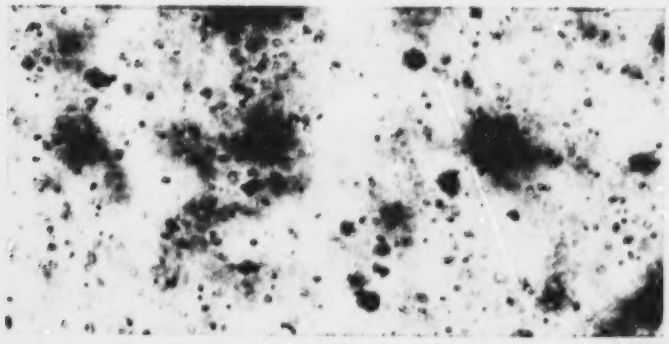

400X

b. Doped at 10^6 particles/cc

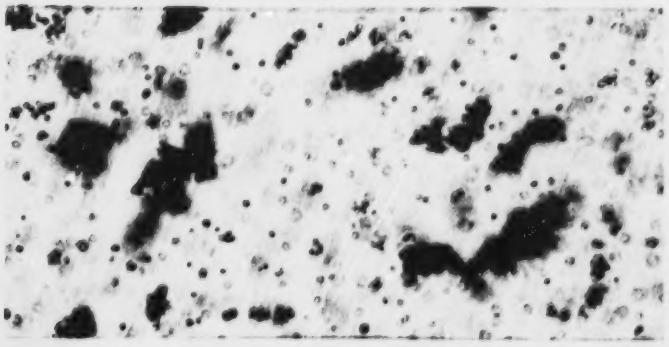

400X

c. Doped at 10^9 particles/cc

Figure 2.4. Photomicrographs of thin sections of RuO_2-doped MCC 76-68.

BEST COPY AVAILABLE

Table 2.2. Results of crystallinity experiment.

Point[a]	Coordinates	T, C	t, hours	log N log (number/cc)	Condition	Crystallinity[b] Surface	Crystallinity[b] Bulk
1	(0, 0, 0)	700	24	7.5	Slumped	L	U
2	(-1, -1, -1)	610	12	6.6	Glazed	N	N
3	(1, -1, -1)	790	12	6.6	Flowed	M	U
4	(-1, 1, -1)	610	36	6.6	Glazed	VL	U
5	(1, 1, -1)	790	36	6.6	Flowed	H	L-M
6	(-1, -1, 1)	610	12	8.4	Glazed	N	U
7	1, -1, 1)	790	12	8.4	Flowed	H	L-M
8	(-1, 1, 1)	610	36	8.4	Glazed, slumped	N	U
9	(1, 1, 1)	790	36	8.4	Flowed	VH	M
10	(-1.68, 0, 0)	550	24	7.5	Unchanged	N	U
11	(1.68, 0, 0)	850	24	7.5	Flowed	N	U
12	(0, -1.68, 0)	700	4	7.5	Flowed, glazed	VL	U
13	(0, 1.68, 0)	700	44	7.5	Flowed	L	U
14	(0, 0, -1.68)	700	24	6	Slumped	M	U
15	(0, 0, 1.68)	700	24	9	Flowed	M	L

(a) The "points" represent the position of the indicated variables in the overall experimental design, shown in Figure 2.5.
(b) N = none; L = light; M = moderate; H = heavy; U = unable to visually determine; V = very.

groundwater constituents but whose effects on glass leaching have, to our knowledge, not yet been experimentally addressed.

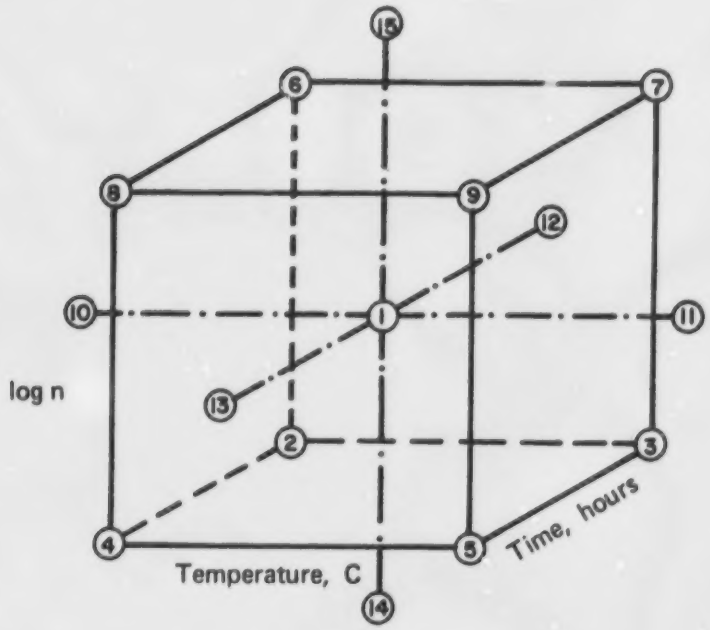

Figure 2.5. Coordinates and levels of central composite design.

Natural organic acids in deep groundwaters may include compounds with a wide range of compositions. We have chosen to evaluate two species that typify two groups of organic acids frequently encountered in the natural environment: acetic acid and humic acid. Acetic acid is one of the principal microbiological breakdown products of numerous natural organic compounds. It occurs widely in oil field waters[2.3] and has recently been identified in deep groundwaters from the Palo Duro Basin, Texas[2.4]--one of the sites recently selected as a potential high-level nuclear-waste repository.

BEST COPY AVAILABLE

Acetic acid was found in concentrations ranging up to 225 mg/liter in Palo Duro groundwaters, along with other short-chain aliphatic acid anions such as propionate, n- and iso-butyrate, and n-valerate, which were present in concentrations up to 23 mg/liter. In oil-field brines, acetic acid concentrations can range to more than 4,000 mg/liter[2.3]. Humic species form mainly in soils and swamps and occur widely in surface and shallow groundwaters and occasionally in deep groundwaters. For example, fulvic acid (a slightly more oxygenated form of humic acid) has been identified in concentrations ranging up to 20 mg/liter in deep groundwaters from the Finnsjon and Sterno areas of Sweden, both of which are prospective radioactive-waste disposal sites in granitic media[2.5].

Thus, acetic acid and humic acid are representative of the types of natural organic compounds that may occur in groundwaters in basaltic lithologies--humic acid because soils and associated vegetation are frequently buried by basalt flows, and acetic acid because it is one of the principal breakdown products of more complex organic compounds. Acetic and humic acids are also appropriate selections for testing because they represent limiting ranges of metal-complexing capacities for natural organic ligands. Acetic acid is a monodentate ligand with relatively weak metal-complexing capacity, and humic acid is a complex polydentate ligand with strong metal-binding characteristics.

The concentrations of organic ligands to be used in the glass-corrosion experiments are intended to bracket the extremes of their expected concentrations in the actual waste-disposal environment. For acetic acid, concentrations of 200 and 2,000 mg/liter are appropriate. To evaluate possible nonlinearity of concentration influences, the geometric mean of the concentrations will also be used--632 mg/liter. Humic acid values will be an order of magnitude lower in all cases, i.e., 20, 63.2, and 200 mg/liter. To our knowledge, the radiation stabilities of these organic compounds are not clearly understood. Similar organic acids, such as EDTA (ethylenediaminetetraacetic acid), have been reported to decompose partially when exposed to intense radiation fields and high temperatures[2.6]. However, the present experiments are intended to simulate glass/water interactions after package failure, which is not expected to occur until thousands of years after disposal when the radiation field surrounding the waste has diminished significantly.

The test plan, which was initiated late in this reporting period, is to dope simulated Grande Ronde basalt water with the required concentrations of humic acid and acetic acid. This doped water will be used in the modified MCC-1P test[2.1]. Chemical analyses of radioactive simulants released to the leachant and surface analyses will be used to evaluate the influences of these two acids. Table 2.3 is a summary of the test.

Table 2.3. Organic acid test conditions.

Dopant[a]	Dopant Concentration (mg/l)	Purpose	Replicates
None	--	Reference	XX
Acetic Acid	200	Low	XX
	632	Middle	XX
	2000	High	XX
Humic Acid	20	Low	XX
	63.2	Middle	XX
	200	High	XX

(a) Added to simulated Grande Ronde basalt groundwater.

2.4 Water Chemistry and Waste-Form Dissolution Modeling

The objective of the waste-form modeling studies is to identify the parameters of groundwater composition that may influence waste-form dissolution. Earlier in the program, two separate modeling efforts were undertaken: the water-chemistry model, dealing with changes in groundwater chemistry near the waste package; and the glass-dissolution model, dealing with the kinetics of glass waste-form dissolution and reprecipitation. Taken together, these two models will help provide a base of information for evaluating the long-term performance of glass waste forms after disposal.

During the past year, efforts have been undertaken to fully integrate the water-chemistry model with the model for waste-form dissolution. The dissolution model that has been used to accomplish this task is based on the following assumptions:

- Glass dissolution occurs congruently and is limited by the rate at which silicon dissolves.
- No spatial variation of the silicon concentration in the groundwater around the glass exists.
- The instantaneous rate of glass dissolution is proportional to the difference between the saturation concentration of silicon in aqueous solution, with respect to the glass, and its actual concentration.

BEST COPY AVAILABLE

- The solution into which the glass dissolves occupies a constant, closed volume.

During the past quarter, efforts were directed toward a more detailed evaluation of this model. It was found, for example, that this general approach to describing the kinetics of heterogeneous reactions has actually been in use for many years, a review of some of the very early studies having been presented by Moelwyn-Hughes[2.7]. More recently, the specific problem of leaching of nuclear-waste-containing glasses has been addressed[2.8,2.9], with varying degrees of complexity, using a glass-dissolution model of this basic type.

The model currently in use does present a simplified view of glass-dissolution kinetics. However, for present purposes, this is actually an advantage, because water-chemistry contributions to glass dissolution can be most easily and explicitly assessed if a relatively simple dissolution model is used, at least initially. Progression to more complex models can then follow.

Studies have already been undertaken in which the model has been generalized to include either a flow-induced exchange of water with the surroundings or the reprecipitation of dissolved glass as a more stable mineral (e.g., quartz). Water-chemistry considerations have not yet, however, been included in these studies.

During the past quarter a manuscript was prepared for submission for publication. In this article, the water-chemistry model and glass-dissolution models are described in detail, and some representative calculations are described relative to effects of water chemistry on the rate of glass dissolution. Another manuscript was prepared in which some of the earlier modeling studies conducted under this program, relative to the kinetics of glass crystallization, are discussed.

During the final quarter of the current funding year, efforts in water-chemistry and glass-dissolution analyses will be directed toward initial studies of chemical species (e.g., certain iron-containing species) that may, if present, enhance the glass-dissolution rate.

2.5 References for Section 2

(2.1) D. Stahl and N. E. Miller (Compilers), "Long-Term Performance of Materials Used for High-Level Waste Packaging", NUREG/CR-3900, Vol. 2 (January 1985), pp. 2-1 ff.

(2.2) D. Stahl and N. E. Miller (Compilers), "Long-Term Performance of Materials Used for High-Level Waste Packaging", NUREG/CR-3900, Vol. 2 (January 1985), pp. 2-23 ff.

BEST COPY AVAILABLE

(2.3) W. W. Carothers and Y. K. Kharaka, "Aliphatic Acid Anions in Oil-Field Waters - Implications for Origin of Natural Gas", American Association of Petroleum Geologists Bulletin, Vol. 62, No. 12, (1978), 2441-2453.

(2.4) J. L. Means and N. J. Hubbard, "The Organic Geochemistry of Deep Ground Waters from the Palo Duro Basin, Texas: Implications for Radionuclide Complexation, Ground Water Origin, and Petroleum Exploration", prepared by Battelle's Columbus Laboratories for the Office of Nuclear Waste Isolation, Battelle Memorial Institute, Columbus, Ohio (in review).

(2.5) J. L. Means, "The Organic Geochemistry of Deep Ground Waters", ONWI-268, prepared by Battelle's Columbus Laboratories for the Office of Nuclear Waste Isolation, Battelle Memorial Institute, Columbus, Ohio (1982).

(2.6) S. N. Bhattacharyya and K. P. Kandu, "Radiolysis of Aqueous Solutions of Nickel (II) EDTA", Radiation Research, Vol. 51 (1972), 45-55.

(2.7) E. A. Moelwyn-Hughes, The Kinetics of Reactions in Solution, 2nd Edition (Oxford University Press, London, 1947), pp. 367 ff.

(2.8) W. L. Kuhn, R. D. Peters, and S. A. Simonson, Nucl. Technol. 63 (1983), 82.

(2.9) K. B. Harvey, Nucl. Chem. Waste Manag. 4 (1983), 201.

BEST COPY AVAILABLE

3. CONTAINER MATERIALS

Studies of overpack corrosion focused on potentiodynamic polarization studies, slow-strain-rate tests, and pitting-kinetics tests in the carbon steel--basalt system. In the potentiodynamic polarization studies, all the species tested, with the exceptions of perchlorate and hydrogen, had a major effect on at least one polarization parameter, indicating that they may influence stress-corrosion cracking behavior. In addition, several of the two-factor interactions were found to be significant in affecting the polarization behavior, and thus synergistic effects of groundwater species on stress-corrosion cracking may exist. In slow-strain-rate studies, specimens tested in 0.0005 M $FeCl_3$ (about 50 ppm Cl^-, which is well below the chloride concentration expected in groundwaters) exhibited about the same susceptibility to cracking as the specimens tested earlier in 0.001 M $FeCl_3$. A study of the effect of temperature on stress-corrosion cracking in 0.0005 M $FeCl_3$ indicated significant cracking over the range 250-315 C. The results of the pitting-kinetics tests indicate that pit propagation occurs readily on 1018 carbon steel in aerated basalt groundwater at 90 C, but rates of propagation are low in comparison to the canister design life.

Fracture-toughness tests were performed on commercial-purity iron to determine its susceptibility to hydrogen embrittlement. The iron samples studied were subject to rapid cracking both in hydrogen and in the nitrogen reference environment. However, hydrogen promoted steady cracking prior to the characteristic rapid cracking, possibly indicating sensitivity to sustained-load subcritical-crack growth.

In the corrosion-correlation effort, the general-corrosion correlation was changed to incorporate a finite rate of film growth; this change will ultimately allow quantitative assessment of the relative importance of diffusion in the solution and growth of the oxide film. The pitting correlation was analyzed in light of the results of the experimental studies of pit growth.

3.1 External Corrosion

During this quarter, studies of overpack corrosion have focused on three areas: potentiodynamic polarization studies, slow-strain-rate studies, and pitting-kinetics studies. All of the studies have dealt with the carbon steel--basalt rock system, but the results of the potentiodynamic polarization studies may be applicable to other hard rock repositories since a broad range of environmental variables is being considered. The objective of the potentiodynamic polarization studies is to evaluate the influence of groundwater chemistry on the potential for stress-corrosion cracking (SCC) and pitting. The slow-strain-rate studies are designed to confirm the results of electrochemical studies with regard to SCC and to investigate the effect of electrochemical potential, temperature, and composition in detail for the identified cracking agents. Pitting-kinetics studies are examining the effects of geometrical and environmental variables on pit propagation.

BEST COPY AVAILABLE

3.1.1 Potentiodynamic Polarization Studies

In this task, potentiodynamic polarization techniques are being used with a statistical experimental design to determine the effects of chemical species on the electrochemical behavior of overpack materials. Fifteen species that are in basalt groundwaters or that are possible radiolysis products have been selected for study. The tests presented in this quarterly report are a matrix of screening experiments to determine which of the fifteen species significantly affect the corrosion of 1020 carbon steel in simulated basalt groundwaters. After the screening tests have been completed, a main matrix of experiments will be performed to quantify the effect of each of the significant species and to examine selected two-factor interactions between the significant species.

3.1.1.1 Experimental Effort

As explained in the most recent annual report,(3.1) in the polarization procedure the polarity and magnitude of the current density between a specimen of the material of interest and an inert counter electrode are measured as a function of electrochemical potential. For the anodic portions of the curve, the current measured is equal to the corrosion rate of the specimen if two conditions are met: (1) the electrochemical potential is sufficiently far away from the open-circuit potential that the rate of the cathodic reaction is negligible; and (2) the rates of parasitic oxidation reactions are negligible.

Schematics of anodic polarization curves showing several types of behavior are given in Figure 3.1. For the active-corrosion case, the anodic curve is linear on an E-log i plot, and the forward and reverse scans are coincident. The presence of a nose in the anodic portion of the curve generally indicates the onset of passivation. The value of the peak current decreases with decreasing potential scan rate and may be negligibly small for a highly corrosion-resistant material. The occurrence of hysteresis between the forward and reverse scans is indicative of pitting. Where the hysteresis loop is very large, the protection potential may be very close to the open-circuit potential, indicating a high probability of pitting in service.

The potentiodynamic polarization technique has been found to be useful in identifying potential SCC environments. For carbon steels, SCC is associated with environments that promote active-passive behavior, and the electrochemical potential range for SCC is near to and more noble than E_{max}. Moreover, severe cracking has been observed in environments when i_{max} on the fast scan is greater than about 1×10^{-3} A/cm^2 and when the fast scan exhibits currents at least an order of magnitude higher than the slow scan. In this program, the following parameters from the polarization curves were selected and analyzed: i_{corr}, E_{corr}, i_{pas}, E_{pit}, E_{prot}, and i_{max} (selected from fast-scan curve).

BEST COPY AVAILABLE

The fifteen species selected for examination in the screening design are given in Table 3.1. In general, these species either are present in the basalt groundwater solutions or are possible radiolysis products. The high concentrations were chosen to demonstrate an effect; they may not necessarily be realistic in all instances, although some of the species may concentrate to these values by local boiling, localized corrosion, or radiolysis. Subsequent tests will be performed at intermediate concentrations to permit interpolation of the data.

The polarization behavior of the candidate alloys was determined using conventional polarization techniques. The specific polarization equipment used for these experiments included a PAR model 173 potentiostat with an ECO Model 567 function generator, coupled to a computer data-acquisition system. A three-compartment electrochemical cell was employed that utilized a saturated calomel reference electrode (SCE) and a platinum counter electrode. All potentials discussed here were measured with respect to the calomel reference electrode. The three-compartment electrochemical cell separates the working electrode from the counter electrode, preventing mixing of the solutions in the counter-electrode and the working-electrode compartments. The working-electrode specimens, hot-rolled 1020 carbon steel, were cylindrical rods drilled and tapped at both ends and sealed off using TEFLON* gaskets. The specimens were typically 0.6 cm in diameter and 1.9 cm in length; the actual area of each specimen was measured prior to immersion in the electrochemical cell. The electrodes were polished with successively finer grades of silicon carbide paper, finishing with a 600-grit grade.

Prior to testing, the working electrode remained in the test solution overnight while the solution was sparged with the desired gas mixture. The polarization scans were then performed approximately 16 hours after immersion of the working electrode in the cell. Partial cathodic and full anodic polarization curves were obtained by scanning at a rate of 0.6 V/h and beginning the scan approximately 100 mV more negative than the free-corrosion potential. The current for the anodic curve was scanned until a current density of approximately 3×10^{-3} A/cm^2 was attained; the potential scan was then reversed until repassivation occurred and the current changed polarity, becoming cathodic. At the completion of the polarization curve, a new steel specimen was inserted into the polarization cell and immediately polarized to a potential of approximately -0.90 V SCE. Within five minutes of immersion, a fast anodic scan was performed using a potential scan rate of 18 V/h.

After completion of the polarization scans, the following polarization parameters were obtained from the polarization curves of potential (E) versus logarithm of current (log i); i_{cor}, E_{cor}, i_{pas}, E_{pit}, E_{prot}, and i_{max} (obtained from fast scan curve).

---

*TEFLON is a registered trademark of the E. I. DuPont de Nemours Company.

BEST COPY AVAILABLE

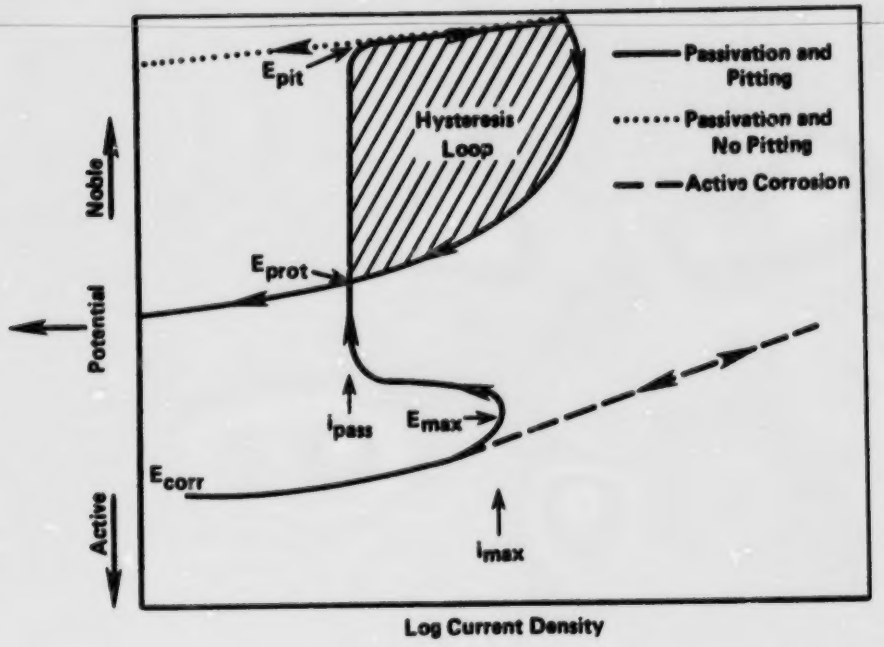

Figure 3.1. Schematic of typical anodic potentiodynamic polarization curves.

E_{cor} = corrosion potential; E_{pit} = potential at which pits initiate on forward scan; E_{prot} = potential at which pits repassivate on reverse scan; i_{max} = current density at active peak; i_{pass} = current density in passive range.

BEST COPY AVAILABLE

Table 3.1 High and low concentrations of species selected for evaluation in the electrochemical experiments

	Species	High Concentration	Low Concentration
1.	pH	9.3	6.0
2.	Cl^{-1}	100,000 ppm	100 ppm
3.	F^{-1}	10,000 ppm	10 ppm
4.	Fe^{+2}/Fe^{+3}	100 ppm	0.05 ppm
5.	Al^{+3}	1,000 ppm	0.1 ppm
6.	CO_3^{-2}/HCO_3^{-1}	1M	0.001 M
7.	NO_3^{-1}/NO_2^{-1}	1,000 ppm [N]	0.1 ppm [N]
8.	PO_4-3	1,000 ppm [P]	0.1 ppm [P]
9.	$BO_3^{-3}/B_4O_7^{-2}$	1,000 ppm [B]	1 ppm [B]
10.	SiO_3^{-2}	1,000 ppm [Si]	10 ppm [S]
11.	H_2O_2	100 ppm	0
12.	ClO_4^{-1}	100 ppm	0
13.	O_2	2% (Vapor)	0
14.	CO	1% (Vapor)	0
15.	H_2	80% (Vapor)	1%

3.1.1.2 Statistical Methodology

To be able to estimate the main effects of each of the fifteen species, a statistical design was used to define the optimal compositions of the test solutions. The statistical design was a partial factorial design of resolution IV. This design permits the main-effect terms of the fifteen variables to be estimated free and clear of other main-effect terms and of any two-factor interactions. Three-factor and greater interactions still confound the main-effect terms; however, these usually contribute only a small response compared to the main-effect-term response. Consequently, a good estimate of the main-effect terms could be calculated at the end of the screening matrix of experiments. Table 3.2 gives the design matrix for the 32 test solutions used in the screening matrix. The pluses and minuses refer to the high and low concentration values given in Table 3.1, respectively. In addition, four experiments were performed using the midpoint of each species concentration to provide an estimate of error for the polarization experiments.

BEST COPY AVAILABLE

Table 3.2. Partial factorial design to be used for the potentiodynamic polarization screening tests.*

Variable	X_1 pH	X_2 Cl	X_3 F	X_4 Fe	X_5 Al	X_6 CO_3/HCO_3	X_7 NO_3/NO_2	X_8 PO_4	X_9 BO_3/B_4O_7	X_{10} SiO_3	X_{11} H_2O_2	X_{12} ClO_4	X_{13} O_2	X_{14} CO	X_{15} H_2
Experiment															
1	-	-	-	-	+	+	+	+	+	+	-	-	-	-	+
2	+	-	-	-	-	-	-	+	+	+	+	+	+	-	-
3	-	+	-	-	-	+	+	-	-	+	+	+	-	+	-
4	+	+	-	-	+	-	-	-	-	+	-	-	+	+	+
5	-	-	+	-	+	-	+	-	+	-	+	-	+	+	-
6	+	-	+	-	+	+	-	-	+	-	-	+	-	+	+
7	-	+	+	-	-	-	+	+	-	-	-	+	+	-	+
8	+	+	+	-	+	+	-	+	-	-	+	-	-	-	-
9	-	-	-	+	+	+	-	+	-	-	-	+	+	+	-
10	+	-	-	+	-	-	/	+	-	-	+	-	-	+	+
11	-	+	-	+	-	+	-	-	+	-	+	-	+	-	+
12	+	+	-	+	+	-	+	-	+	-	-	+	-	-	-
13	-	-	+	+	+	-	-	-	-	+	+	+	-	-	+
14	+	-	+	+	-	+	+	-	-	+	-	-	+	-	-
15	-	+	+	+	-	-	-	+	+	+	-	-	-	+	-
16	+	+	+	+	+	+	+	+	+	+	+	+	+	+	+
17	+	+	+	+	-	-	-	-	-	-	+	+	+	+	-
18	-	+	+	+	+	+	+	-	-	-	-	-	-	+	+
19	+	-	+	+	+	-	-	+	+	-	+	+	-	+	+
20	-	-	+	+	-	+	+	+	+	-	+	-	-	-	-
21	+	+	-	+	-	+	-	+	-	+	-	+	-	-	+
22	-	+	-	+	+	-	+	+	-	+	+	-	+	-	-
23	+	-	-	+	+	+	-	-	+	+	+	-	-	+	-
24	-	-	-	+	-	-	+	-	+	+	-	+	+	+	+
25	+	+	+	-	-	-	+	-	+	+	+	-	+	-	+
26	-	+	+	-	+	+	-	-	+	+	-	+	-	-	-
27	+	-	+	-	+	-	+	+	-	+	-	+	-	+	-
28	-	-	+	-	-	+	-	+	-	+	+	-	+	+	+
29	+	+	-	-	-	+	+	+	+	-	-	-	+	+	-
30	-	+	-	-	+	-	-	+	+	-	+	+	-	+	+
31	+	-	-	-	+	+	+	-	-	-	+	+	+	-	-
32	-	-	-	-	-	-	-	-	-	-	-	-	-	-	-
33	MIDPOINTS														

*+ and - refer to the high and low concentrations, respectively, indicated in Table 3.1.

At the completion of the screening matrix of experiments, a regression analysis was performed on the different corrosion parameters with the aid of a multiple regression routine on the MINITAB statistical computer program.* The regression analysis calculated the "F" ratio and the regression coefficient for each of the fifteen species. The "F" statistic is a ratio of two variances, i.e., the sum of squares explained by each factor when entered in the equation, divided by the residual mean square (error). In general, when the calculated "F" ratio for a factor is large, it means that a large amount of experimental variation is explained by this term compared to the error variation. If a calculated "F" ratio exceeds the appropriate tabulated "F" value, then it can be assumed that the solution variable has a statistically significant effect on a particular polarization parameter. A 90-percent probability that a species is significant is usually acceptable for most experimental work and implies that one accepts a 10-percent chance of being wrong in assuming that the factor has a significant effect.

The regression coefficients are multiplicative terms for the factors in a regression equation and were determined by a linear least square fit of the data. The regression coefficients determined in this study are calculated based on the high and low concentrations (+1 and -1) of the various chemical species. These factors are based on the design concentration range of the species indicated in Table 3.1. Because precipitation occurred in several solutions, the actual concentrations achieved in the test solutions were not the designed values. Therefore, the regression coefficients provide relative magnitudes of the measured effects only and are not meant to give a quantitative measure of the effects. Solutions are in the process of being analyzed, and actual chemical concentrations of the species examined will be used in the final analysis to provide the quantitative measure for the regression coefficients.

3.1.1.3 Results

Polarization experiments were performed in each of the 33 solutions given in Table 3.2. Figures 3.2 to 3.4 show polarization curves obtained in solutions 11, 14, and 30 respectively. These polarization curves show the wide range of behavior observed by varying the concentration of the 15 species in the screening matrix of experiments. The polarization parameters selected from the curves also are shown in the figures. As can be seen, all of the polarization parameters cannot be selected from each curve. For example, Figure 3.4 shows no passive behavior and therefore i_{pas}, E_{pit}, and E_{prot} were not selected for this solution. Table 3.3 shows the values for the polarization parameters for all 33 solutions that were used in the statistical analysis. The variations in the polarization parameters for the four tests repeated for solution 33 gives an indication of the reproducibility of the data obtained.

---

*Minitab Project, Statistics Department, 215 Pond Laboratory, The Pennsylvania State University, University Park, PA, 16802, 1981.

BEST COPY AVAILABLE

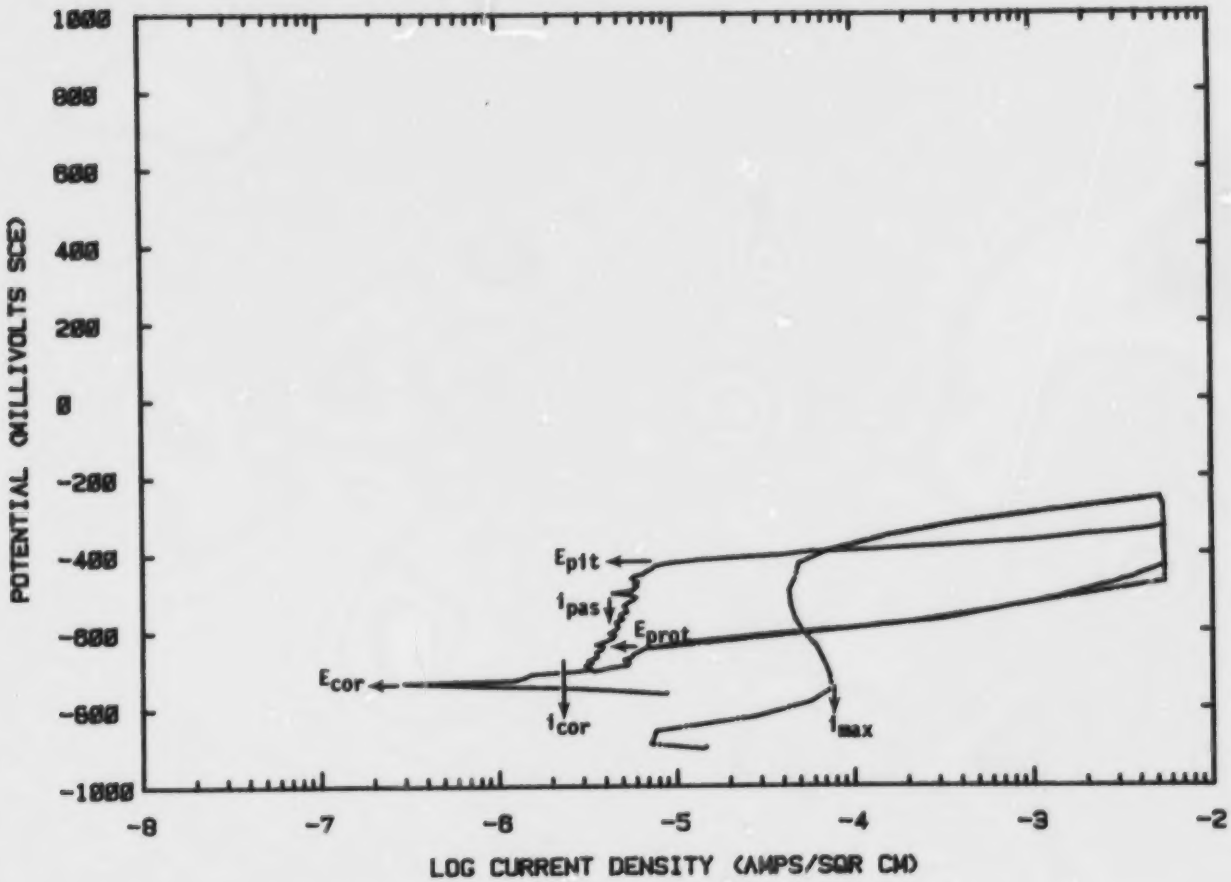

Figure 3.2. Potentiodynamic polarization curves for 1020 carbon steel in solution 11.

See Table 3.2 for solution composition.

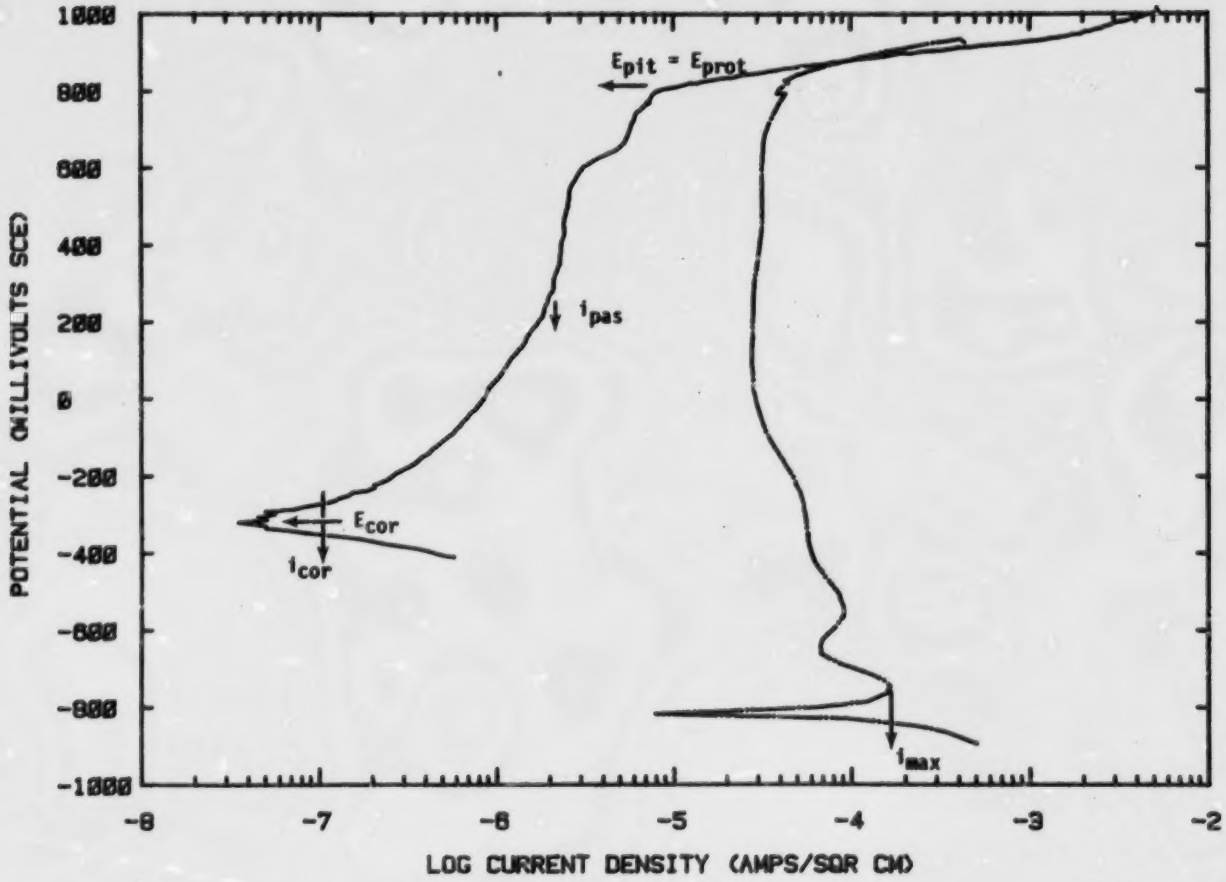

Figure 3.3. Potentiodynamic polarization curves for 1020 carbon steel in solution 14.

See Table 3.2 for solution composition.

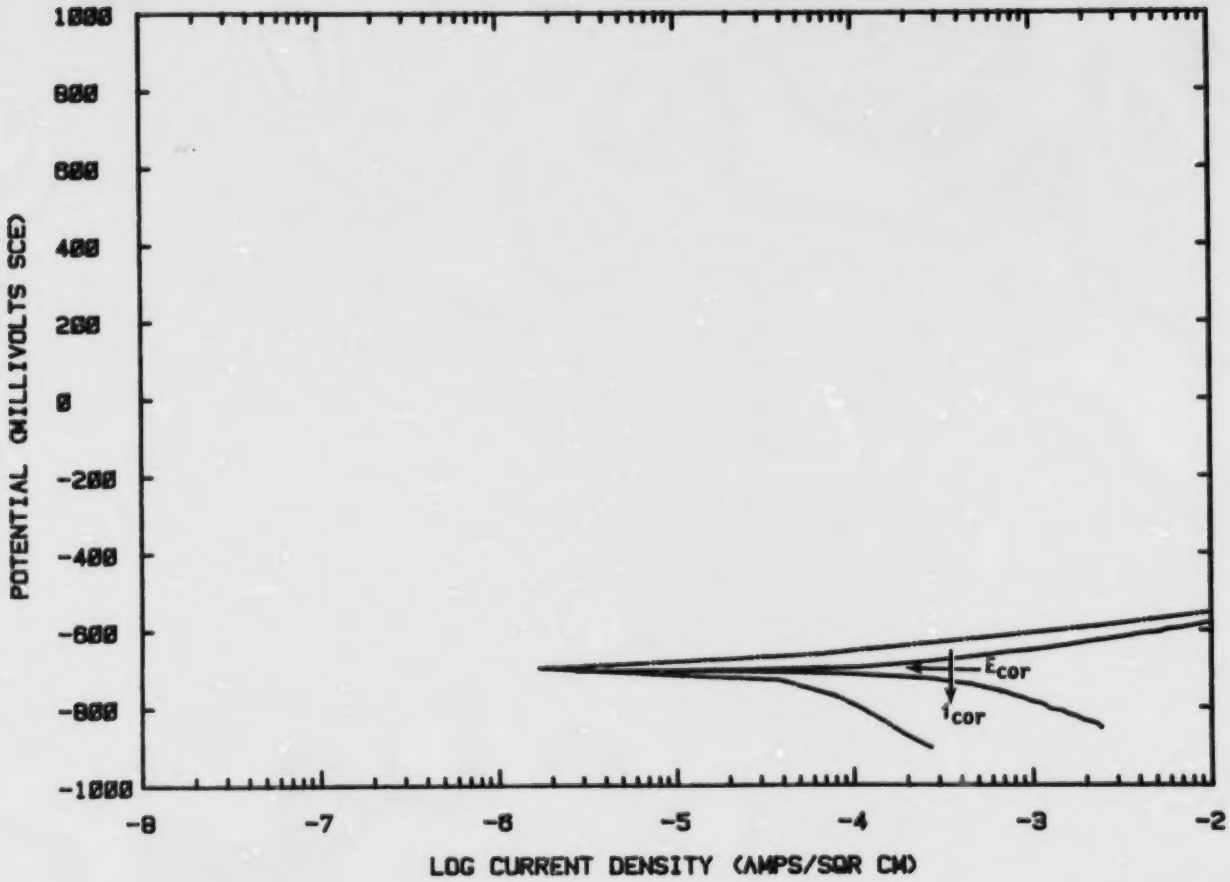

Figure 3.4. Potentiodynamic polarization curves for 1020 carbon steel in solution 20.

See Table 3.2 for solution composition.

Table 3.3. Experimentally-measured polarization parameters for the 33 test solutions defined in Table 3.2.

Solution	i_{cor} A/cm^2	E_{cor}, V(SCE)	i_{pas}, A/cm^2	E_{pit}, V(SCE)	E_{prot}, V(SCE)	$i_{max(fast)}$, A/cm^2
1	7.78×10^{-6}	-.422	2.21×10^{-5}	-.254	-.527	4.32×10^{-4}
2	2.0×10^{-7}	-.2	3.01×10^{-6}	.776	.776	2.23×10^{-5}
3	1.0×10^{-6}	-.574	4.61×10^{-6}	-.461	-.593	1.26×10^{-5}
4	7.32×10^{-7}	-.767	*	-.576	-.718	1.37×10^{-5}
5	1.0×10^{-4}	-.325	7.84×10^{-4}	1.0	1.0	1.87×10^{-3}
6	1.57×10^{-4}	-.859	8.97×10^{-5}	.808	-.808	2.46×10^{-3}
7	7.44×10^{-5}	-.515	9.33×10^{-4}	-.20	-.544	1.94×10^{-4}
8	4.21×10^{-5}	-.891	2.29×10^{-5}	-.042	-.625	1.57×10^{-3}
9	1.38×10^{-5}	-.781	1.30×10^{-5}	-.562	-.657	9.84×10^{-5}
10	1.1×10^{-6}	-.20	2.63×10^{-6}	.557	-.261	1.27×10^{-5}
11	2.97×10^{-6}	-.735	5.25×10^{-6}	-.422	-.64	7.49×10^{-5}
12	5.44×10^{-6}	-.623	2.73×10^{-5}	-.471	-.547	2.4×10^{-5}
13	5.74×10^{-5}	-.461	7.78×10^{-5}	-.33	-.471	7.5×10^{-4}
14	1.0×10^{-7}	-.31	2.42×10^{-6}	.808	.808	1.66×10^{-4}
15	8.51×10^{-5}	-.725	4.05×10^{-5}	-.557	-.64	1.37×10^{-4}
16	9.19×10^{-7}	-.515	2.73×10^{-6}	.54	-.452	1.32×10^{-4}
17	6.05×10^{-6}	-.657	1.11×10^{-5}	-.483	-.718	4.9×10^{-5}
18	8.97×10^{-6}	-.625	*	-.466	-.576	6.64×10^{-5}
19	5.83×10^{-6}	-.435	2.33×10^{-6}	.825	.776	5.24×10^{-5}
20	8.58×10^{-5}	-.498	1.32×10^{-4}	-.247	-.608	2.09×10^{-3}
21	2.03×10^{-6}	-.94	1.51×10^{-5}	.588	-.342	6.2×10^{-3}
22	5.08×10^{-5}	-.576	1.96×10^{-4}	-.42	-.515	5.30×10^{-5}
23	3.25×10^{-5}	-.876	6.53×10^{-5}	.745	.745	8.64×10^{-3}
24	2.12×10^{-6}	-.31	8.58×10^{-6}	.80	-.088	3.50×10^{-4}
25	6.0×10^{-6}	-.657	4.44×10^{-5}	-.40	-.576	2.73×10^{-5}
26	1.09×10^{-6}	-.64	*	-.483	-.718	1.49×10^{-4}
27	1.6×10^{-7}	-.562	7.38×10^{-7}	.083	-.53	4.08×10^{-5}
28	7.26×10^{-4}	-.688	*	*	*	3.33×10^{-3}
29	8.58×10^{-6}	-.562	1.07×10^{-4}	.80	-.042	2.71×10^{-3}
30	3.04×10^{-4}	-.703	*	*	*	*
31	6.43×10^{-4}	-.845	1.52×10^{-4}	.684	.684	3.37×10^{-3}
32	5.49×10^{-6}	-.781	6.25×10^{-6}	-.544	-.657	4.86×10^{-5}
33A	2.5×10^{-6}	-.544	6.25×10^{-6}	-.293	-.576	1.12×10^{-4}
33B	1.1×10^{-6}	-.466	3.73×10^{-6}	-.31	-.576	1.17×10^{-4}
33C	1.37×10^{-6}	-.53	4.27×10^{-6}	-.232	-.576	8.97×10^{-5}
33D	1.48×10^{-6}	-.53	4.61×10^{-6}	-.31	-.576	1.11×10^{-4}

*Not measured from polarization behavior.

BEST COPY AVAILABLE

Results of the statistical analysis performed on the polarization data are given in Table 3.4. These data indicate the main effect for each of the 15 species on the six polarization parameters examined. The "F" value indicates the significance of the species, and the coefficient indicates the relative magnitude of the effect. Coefficients are given only for those species that have a significant effect, based on a 75-percent or greater probability. For the majority of the discussions, a 90-percent or greater probability is typically required before an effect is considered significant. A positive coefficient indicates that an increase in concentration increases the value of the parameter, and a negative coefficient indicates that an increase in concentration of the species decreases the value of the parameter. Table 3.4 indicates that a majority of the species have an effect on at least one of the polarization parameters with the exceptions being perchlorate (ClO_4^-) and hydrogen (H_2), based on a 90-percent or greater probability of significance.

Table 3.5 gives the results of the statistical analysis for the 15 groups of interactions that can be distinguished by the screening matrix design. The purpose of showing this table is to indicate that several of the two-factor interactions of the 15 species being examined are significant. Of particular interest to this program is the fact that several interactions are significant when considering i_{max}, which indicates the tendency for stress-corrosion cracking, and when considering E_{pit} and E_{prot}, which indicate the effects on pitting behavior.

Table 3.6 summarizes the results of the statistical analysis for the main effects of the chemical species examined in the screening tests. Arrows are used to indicate the direction of the effect for each species that had a significant effect, based on a 90-percent or greater probability. Many of the effects were expected, such as O_2 and NO_3 increasing E_{cor} and CO_3^{-2}/HCO_3^- decreasing E_{cor}. Other effects, such as Cl^- decreasing E_{cor}, were not particularly expected but can be explained since Cl^- would tend to make the steel more active and would thereby decrease E_{cor}. It is also noteworthy that several species had a significant effect on i_{pas}. Referring back to Table 3.4, NO_3^-/NO_2^- and $BO_3^{-3}/B_4O_7^{-2}$ had very large coefficients, indicating that these species greatly increased the passive current density with an increase in concentration, while SiO_3^{-2} and CO had large negative coefficients, indicating that these species greatly decreased i_{pas} with an increase in concentration.

The polarization parameter i_{max}, which is the maximum current density during the active peak as measured with the fast scan technique, has been used to indicate the tendency for stress-corrosion cracking. Generally, a higher stress-corrosion cracking tendency is indicated by a larger i_{max}. As expected, CO_3^{-2}/HCO_3^- produced a significant increase in i_{max} with increasing concentrations. Chloride, on the other hand, decreased i_{max} with increasing concentration. This effect was not expected and will be considered more closely in the main matrix of experiments.

BEST COPY AVAILABLE

Table 3.4. Results of statistical analysis indicating the effect of each chemical species on the polarization parameters measured by potentiodynamic polarization.

	E_{cor}		$\log i_{cor}$		$\log i_{max}$		$\log i_{pas}$		E_{pit}		E_{prot}	
	F	Coef	F	Coef	F	Coef	F	Coef	F	Coef	F	Coef
pH	0.5		6.4	-0.34*	0.0		174	-0.18*	27	+0.31*	13	+0.22*
Cl	7.6	-0.06*	0.2		7.1	-0.23*	34	+0.06*	26	-0.25*	30	-0.32*
F	0.5		1.0		1.8	+0.11**	39	-0.08*	0.0		0.3	
Fe	0.9		0.9		0.2		86	+0.41*	0.0		0.3	
Al	1.1		0.8		0.0		36	+0.03*	1.7		0.1	
CO_3/HCO_3	8.4	-0.07*	0.3		25.1	+0.43*	3.6	-0.16**	2.9	+0.06**	0.9	
NO_3/NO_2	15.0	+0.09*	1.1		0.9		19	+0.64*	4.0	+0.13**	0.1	
PO_4	1.1		0.4		0.3		28	+0.10*	0.3		2.6	-0.10**
BO_3/B_4O_7	1.9	+0.03**	0.1		1.3		29	+0.78*	6.0	+0.14*	5.1	+0.13*
SiO_3	1.1		7.2	-0.36*	0.2		138	-0.85*	0.0		0.1	
H_2O_2	0.3		4.2	+0.27*	0.4		16	+0.25*	0.0		0.2	
ClO_4	0.2		0.1		0.0		1.2		0.2		1.3	
O_2	3.9	+0.05*	0.5		0.0		1.3		9.3	+0.13*	8.2	+0.15*
CO	0.1		0.1		0.0		22	-0.64*	1.1		0.0	
H_2	0.0		1.7	+0.17**	0.2		0.3		1.2		0.1	

*Greater than 90 percent probability that effect is significant.
**Greater than 75 percent but less than 90 percent probability that effect is significant.

Table 3.5. Results of statistical analysis indicating the effect of groups of interactions on the polarization parameters measured by potentiodynamic polarization.

	F	E_{cor} Coef	F	$\log i_{cor}$ Coef	F	$\log i_{max}$ Coef	F	$\log i_{pas}$ Coef	F	E_{pit} Coef	F	E_{prot} Coef
ClxAl, $FxCO_3$, $FexNO_3$, $PO_4xH_2O_2$, BO_3xClO_4, SiO_3xO_2, $COxH_2$	1.3		0.6		2.9	-0.14**	61.2	-0.74*	0.0		0.7	
pHxAl, $FxPO_4$, $FexBO_3$, $CO_3xH_2O_2$, NO_3xClO_4, SiO_3xCO, O_2xH_2	3.3	-0.04**	0.3		0.0		144.8	-0.65*	0.1		0.4	
$pHxCO_3$, $ClxPO_4$, $FexSiO_3$, $AlxH_2O_2$, NO_3xO_2, BO_3XCO, ClO_4xH_2	2.1	-0.03**	6.5	+0.33*	24.2	+0.40*	852.6	+1.02	15.6	+0.20*	6.9	+0.15*
$pHxNO_3$, $ClxBO_3$, $FxSiO_3$, $AlxClO_4$, CO_2xO_2, PO_4xCO, $H_2O_2xH_2$	0.2		0.1		2.0	-0.12**	58.1	-0.08*	4.0	-0.13**	6.4	-0.12*
pHxCl, FxH_2O_2, $FexClO_4$, CO_3xPO_4, NO_3xBO_3, SiO_3xH_2, O_2xCO	0.4		0.3		4.8	+0.18*	47.3	-0.49*	2.2	-0.07**	9.1	-0.15*
pHxF, $ClxH_2O_2$, $FexO_2$, $AlxPO_4$, NO_3xSiO_3, BO_3xH_2, ClO_4xCO	0.1		2.3	-0.19**	8.5	-0.24*	53.7	+0.47*	0.8		0.6	
pHxFe, $ClxClO_4$, FxO_2, $AlxBO_3$, CO_3xSiO_3, PO_4xH_2, H_2O_2xCO	1.2		0.4		0.1		3.2	-0.01**	0.8		0.0	
ClxF, $pHxH_2O_2$, $FexCO$, $AlxCO_3$, NO_3xH_2, BO_3xSiO_3, ClO_4xO_2	0		0.1		0.8		136.7	+0.42*	0.7		0.4	
ClxFe, $pHxClO_4$, $FxCO$, $AlxNO_3$, CO_3xH_2, PO_4xSiO_3 $H_2O_2xO_2$	1.3		0.4		0.2		24.9	-0.09*	0.0		0.1	
FxFe, HxO_2, $ClxCO$, $AlxH_2$, CO_3xNO_3, PO_4xBO_3, $H_2O_2xClO_4$	2.0	+0.03**	0.4		2.7	-0.13**	11.2	-0.06*	0.6		0.2	
FxAl, $ClxCO_3$, $pHxPO_4$, $FexH_2$, NO_3xCO, BO_3xO_2, SiO_3xClO_4	5.0	-0.05*	9.9	-0.40*	0.7		7.9	+0.18*	10.5	+0.18*	0.7	
FexAl, $ClxNO_3$, $pHxBO_3$, FxH_2, CO_3xCO, PO_4xO_2, $SiO_3xH_2O_2$	0.1		0.6		0.6		--		0.1		0.5	
$FexCO_3$, $FxNO_3$, $pHxSiO_3$, $ClxH_2$, $AlxCO$, PO_4xClO_4, $BO_3xH_2O_2$	0.2		3.1	-0.23**	0.8		--		--		--	
$FexPO_4$, $FxBO_3$, $ClxSiO_3$, $pHxH_2$, $AlxO_2$, CO_3xClO_4, $NO_3xH_2O_2$	1.6		0.1		0.8		0.01		0.8		1.4	
$FexH_2O_2$, ClO_4xF, O_2xCl, $COxpH$, $AlxSiO_3$, CO_3xBO_3, NO_3xPO_4	0		0.5		0.0		--		0.2		2.3	-0.11**

*Greater than 90 percent probability that effect is significant.
**Greater than 75 percent but less than 90 percent probability that effect is significant.

Table 3.6. Summary of results of statistical analysis for the main effects of the chemical species based on a 90 percent or greater probability of significance.

	E_{cor}	log i_{cor}	log i_{max}	log i_{pas}	E_{pit}	E_{prot}
pH	-	↓	-	↓	↑	↑
Cl	↓	-	↓	↑	↓	↓
F	-	-	-	↓	-	-
Fe	-	-	-	↑	-	-
Al	-	-	-	↑	-	-
CO_3/HCO_3	↓	-	↑	-	-	-
NO_3/NO_2	↑	-	-	↑	-	-
PO_4	-	-	-	↑	-	-
BO_3/B_4O_7	-	-	-	↑	↑	↑
SiO_3	-	↓	-	↓	-	-
H_2O_2	-	↑	-	↑	-	-
ClO_4	-	-	-	-	-	-
O_2	↑	-	-	-	↑	↑
CO	-	-	-	↓	-	-
H_2	-	-	-	-	-	-

BEST COPY AVAILABLE

Pitting behavior also was affected significantly by some of the species. Chloride, as expected, tended to decrease E_{pit} and E_{prot}, indicating more severe pitting conditions. Oxygen, BO_3/B_4O_7 and pH all tended to increase E_{pit} and E_{prot} with increasing concentration.

Based on the results of the statistical analysis, 11 species were selected to be examined in the main matrix of experiments. As shown in Table 3.6, H_2 and ClO_4^- had no effect on the polarization parameters measured, based on a 90-percent or greater probability of significance; therefore, these two species were removed from further consideration. (It should be noted that ClO_4^- may have an effect that lasts for only a short period of time, and that it might have been overlooked in the present experiments. Therefore, it will be proposed that additional work be performed to consider the effects of ClO_4^-.) The other two species that will not be considered in the main matrix of experiments are Al and PO_4^{-3}. Both of these species were removed since they only affected i_{pas} and the coefficients of the effects (see Table 3.4) were less than those of the other species. Fluoride also had only a small effect on i_{pas} but showed an effect on i_{max} with a probability of significance greater than 75 percent but less than 90 percent. The decision, therefore, was made to retain fluoride in the main matrix. Table 3.7 shows the 11 species that will be included in the main test matrix and the 21 two-factor interactions that will also be examined. The interactions included in Table 3.7 were based upon the results presented in Table 3.5 and on experience.

Table 3.7. Main effects and interactions selected from screening tests to be examined in main test matrix.

Main Effects	Two-Factor Interactions	
pH	pH x Cl	Cl x H_2O_2
Cl	pH x CO_3	CO_3 x H_2O_2
F	pH x NO_3	CO_3 x O_2
Fe	pH x BO_3	NO_3 x BO_3
CO_3/HCO_3	pH x SiO_3	NO_3 x O_2
NO_3/NO_2	pH x H_2O_2	NO_3 x SiO_3
BO_3/B_4O_7	pH x O_2	BO_3 x SiO_3
SiO_3	pH x CO	BO_3 x H_2O_2
H_2O_2	Cl x CO_3	SiO_2 x O_2
O_2	Cl x NO_3	H_2O_2 x O_2
CO	Cl x BO_3	

BEST COPY AVAILABLE

During the next quarter, a computer-assisted experimental design will be performed to determine the optimum test matrix to permit the determination of the main-effect terms and the two-factor interactions. Polarization behavior will be determined for 1020 carbon steel in each of the solutions in this test matrix in the same manner as in the screening test matrix reported above.

3.1.2 Slow Strain Rate Studies

In the literature, several species which may be present in the repository were identified as potential stress-corrosion cracking agents. Of these, $FeCl_3$ (or chloride plus ferric oxides or hydroxides) is potentially the most problematic since chlorides are present in the groundwater, and corrosion of the overpack would generate ferrous ions which could be oxidized to ferric ions by radiolysis or oxygen ingress. Strauss and Bloom[3.2] first reported on the stress-corrosion cracking of low-carbon steels by ferric chloride solutions in 1961. Transgranular cracking was observed in pressurized capsule tests at 316 C with very low concentrations (0.001 M) of ferric chloride and in aqueous slurries of FeOOH or Fe_2O_3 and NaCl. On the other hand, NaCl plus Fe_3O_4 did not produce cracking.

Although the stress-corrosion cracking observed by Strauss and Bloom may be relevant to overpack performance, it has not been established whether stress-corrosion cracking of carbon steel will occur at the low temperatures typical of waste repositories or in more complicated aqueous solutions containing typical groundwater species. Moreover, it was not evident from the original reference whether the cracking occurred in the vapor or in the liquid phase within the capsules. Accordingly, an experimental investigation was undertaken to reproduce the stress-corrosion cracking observed in the original reference and to examine the influence of temperature and solution chemistry on stress-corrosion cracking of low-carbon steels in these ferric chloride solutions.

Last reporting period, it was found that cracking of hot-rolled 1020 carbon steel could readily be produced in 0.001 M $FeCl_3$, in the liquid phase, at 315 C. It was also found that the maximum depth of cracking was highest at the slowest strain rate studied, 1×10^{-8}/s, whereas the cracking velocity was highest at the high strain rate because failure times were shorter at the higher strain rates (see Table 3.8). An intermediate strain rate, 1×10^{-7}/s, was selected for subsequent tests.

It was noted that significant general attack occurred on the specimens exposed to the 1×10^{-3} M $FeCl_3$ solution at 315 C (see Figure 3.5) and accordingly, it was speculated that cracking would be at least as severe at lower $FeCl_3$ concentrations. Subsequent specimens tested in 5×10^{-4} M $FeCl_3$ solutions exhibited about the same susceptibility to cracking as those tested in 1×10^{-3} M $FeCl_3$ solutions, but the morphology of the attack was altered by the change in solution concentration. Whereas the cracks in specimens tested in 1×10^{-3} M $FeCl_3$

BEST COPY AVAILABLE

Table 3.8. Summary of results of slow strain rate experiments performed on hot-rolled 1020 carbon steel in $FeCl_3$ solutions.

Strain Rate s^{-1}	Solution Composition M	Temperature C	Maximum Crack Depth mm	Time to Failure hours	Crack Velocity mm/s
1×10^{-8}	1×10^{-3}	315	0.30	393	2.10×10^{-7}
6×10^{-8}	1×10^{-3}	315	0.11	146	2.09×10^{-7}
6×10^{-7}	1×10^{-3}	315	0.20	59.2	9.53×10^{-7}
1×10^{-7}	5×10^{-4}	315	0.28	282	2.75×10^{-7}
1×10^{-7}	5×10^{-4}	275	0.12	165	2.05×10^{-7}
1×10^{-7}	5×10^{-4}	250	0.14	148	2.67×10^{-7}

BEST COPY AVAILABLE

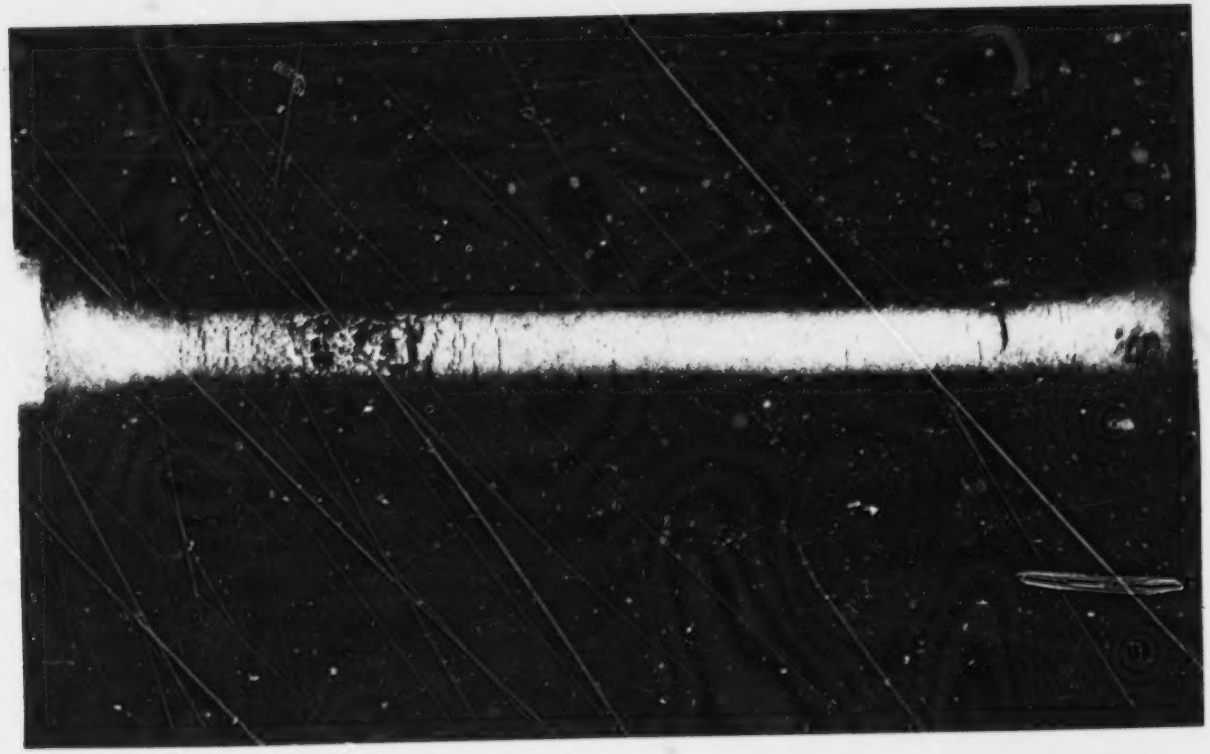

5X 8L139

Figure 3.5. Low-power optical photograph of gauge length of hot-rolled 1020 carbon steel specimen tested in 0.001 M $FeCl_3$ at 315 C at a strain rate of 6×10^{-7}/s.

were generally well defined, with sharp tips, those tested in 5×10^{-4} M $FeCl_3$ exhibited blunt crack tips, as if pitting had initiated at the crack tips (see Figures 3.6 and 3.7). Lower $FeCl_3$ concentrations were not studied since 5×10^{-4} M $FeCl_3$ corresponds to about 50 ppm chloride, which is well below the nominal chloride concentration of basalt groundwater.

The effect of temperature on the stress-corrosion cracking of hot-rolled 1020 carbon steel was studied at 5×10^{-4} M $FeCl_3$ at a strain rate of 1×10^{-7}/sec. The results, summarized in Table 3.8 and Figure 3.8, show that maximum crack depths decrease with decreasing temperature but that the trend in cracking velocity with temperature was less pronounced; measurable cracking was observed at 250 C.

The morphology of the cracking was similar at the three temperatures studied, with blunt crack tips. However, more corrosion products/oxides were present in the cracks at the lower temperatures, as shown in Figures 3.7, 3.9, and 3.10.

3.1.3 Pit-Propagation Experiments

Several electrochemical pit-propagation experiments were performed during the system debugging. These experiments were performed with a pit-propagation monitor which is shown schematically in Figure 3.11. Experimentally, the monitor is oriented vertically in a test cell containing an electrolyte, and the current flow between the base of the simulated pit and the boldly exposed surface is monitored as a function of exposure time. Current measurements provide an estimation of the rate of pit propagation; the rate measured may be somewhat non-conservative since the reduction reactions occurring on the pit base will contribute to pit propagation but will not be detected. This current may be significant where a very-low-pH environment develops within the pit. Results of one of the early experiments, reported last quarter, indicated that consistent occluding of the cell was not achieved readily with normal corrosion processes or through anodic stimulation. Accordingly, it was decided to investigate the effectiveness of two candidate procedures for occluding the cell: (1) packing the pit with an Fe_3O_4 slurry, or (2) plugging the pit mouth with a glass frit. Optical examination of specimens from previous exposures in aerated basalt groundwater indicated that red oxides were present on the outside surfaces of the specimens, but black oxides were adjacent to the metal and attack had occurred beneath the deposits. X-ray diffraction analyses will be performed on both types of deposits, but it is probable that the inner deposit is Fe_3O_4 and the outer deposit is FeOOH or a hydrated form of Fe_2O_3.

The cells were set up with aspect ratios of 3:1 in standard simulated basalt groundwater (pH 9.8). The cells were deaerated with nitrogen at 75 C for 24 hours. Oxygen was then introduced at a flow rate of approximately 10 cc/min, and the galvanic current flow between the inner pits and the boldly exposed surfaces was monitored as a function of time. Pitting was established almost immediately, as indicated by

500X 7L545

Figure 3.6. Optical photographs of metallographic section of hot-rolled 1020 carbon steel specimen tested in 0.001 M $FeCl_2$ at 315 C at a strain rate of 6×10^{-8}/s.

BEST COPY AVAILABLE

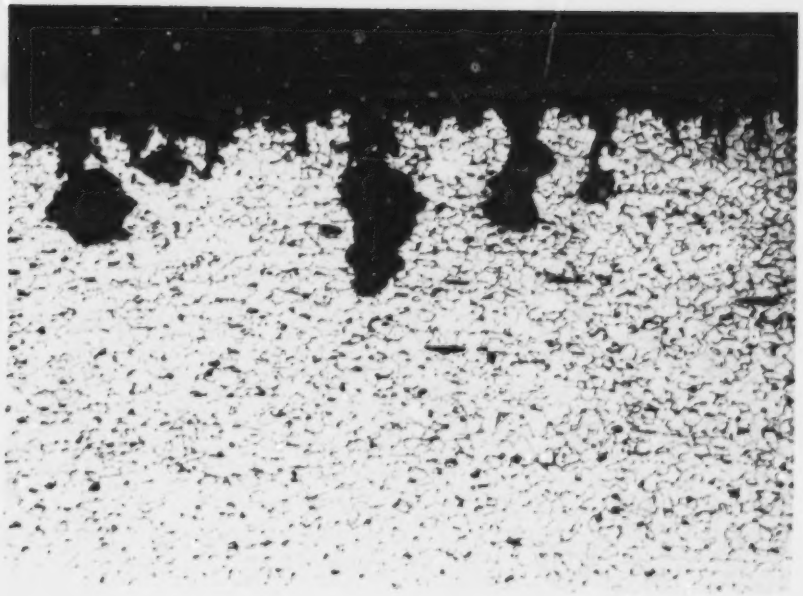

100X 8L343

Figure 3.7. Optical photograph of metallographic section of hot-rolled 1020 carbon steel specimen tested in 0.0005 M $FeCl_3$ at 315 C at a strain rate of 1×10^{-7}/s.

BEST COPY AVAILABLE

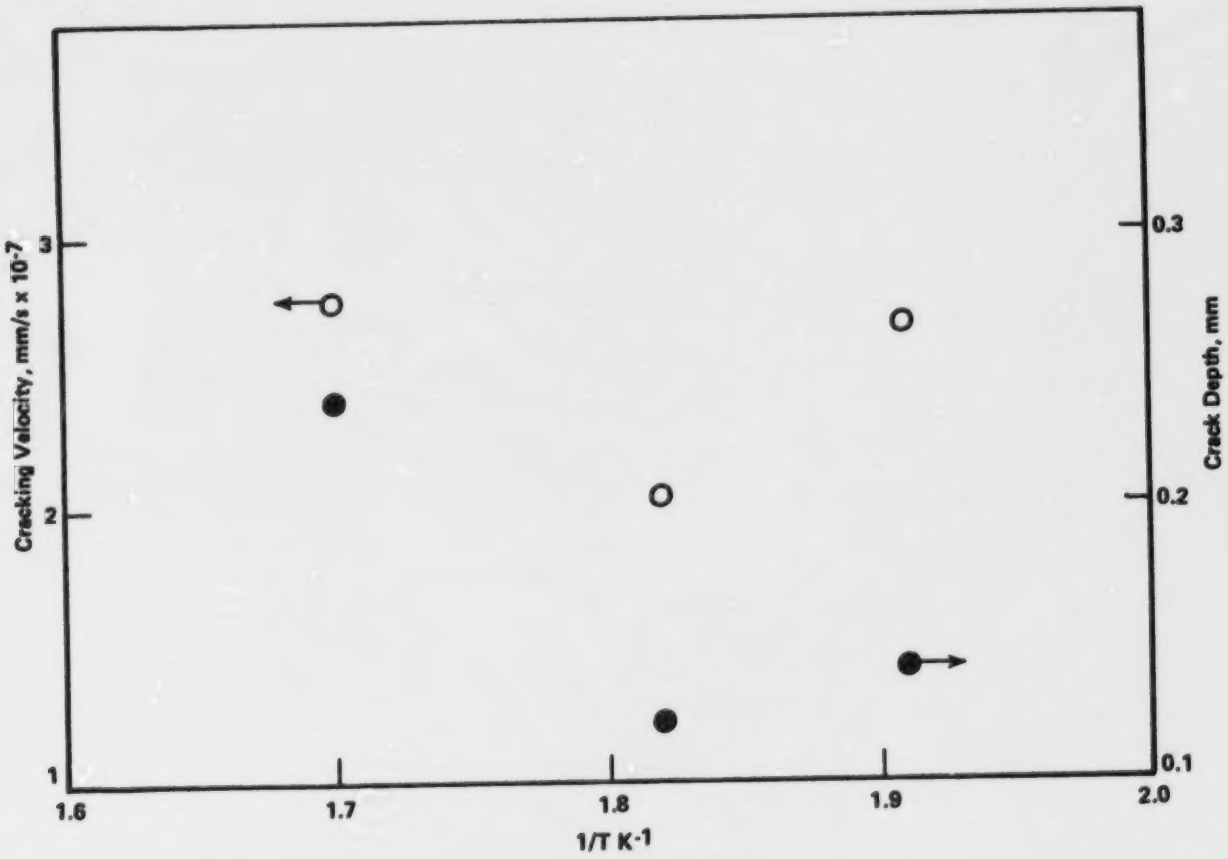

Figure 3.8. Effect of temperature on crack velocity and crack depth for hot-rolled 1020 carbon steel tested in 0.0005 M $FeCl_3$ at a strain rate of 1 x 10^{-7}/s.

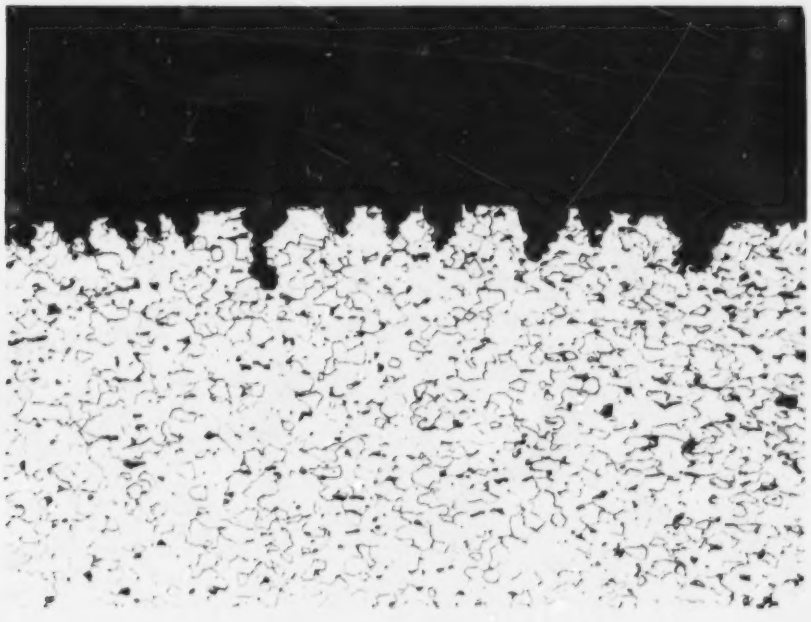

100X 8L626

Figure 3.9. Optical photograph of metallographic section of hot-rolled 1020 carbon steel specimen tested in 0.0005 M $FeCl_3$ at 275 C at a strain rate of 1×10^{-7}/s.

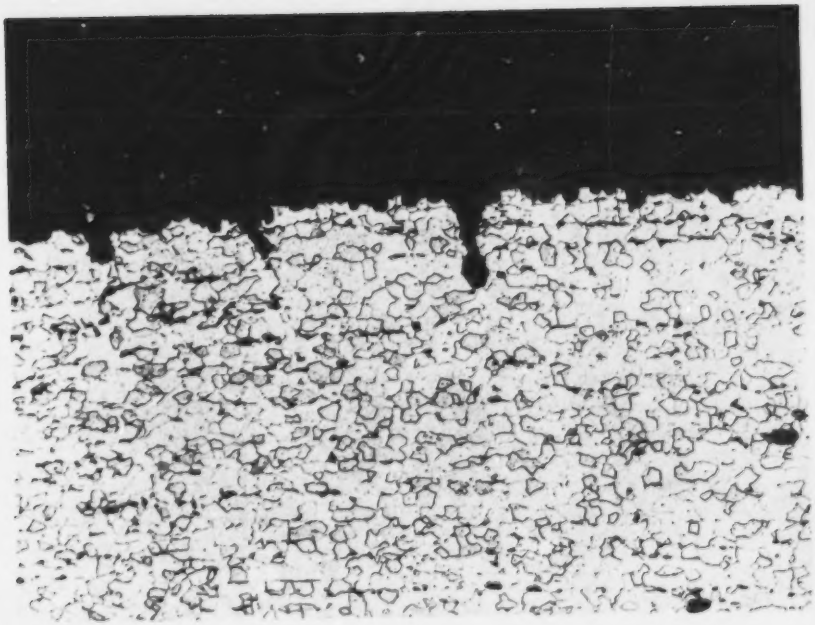

100X 8L811

Figure 3.10. Optical photograph of metallographic section of hot-rolled 1020 carbon steel specimen tested in 0.0005 M $FeCl_3$ at 250 C at a strain rate of 1×10^{-7}/s.

BEST COPY AVAILABLE

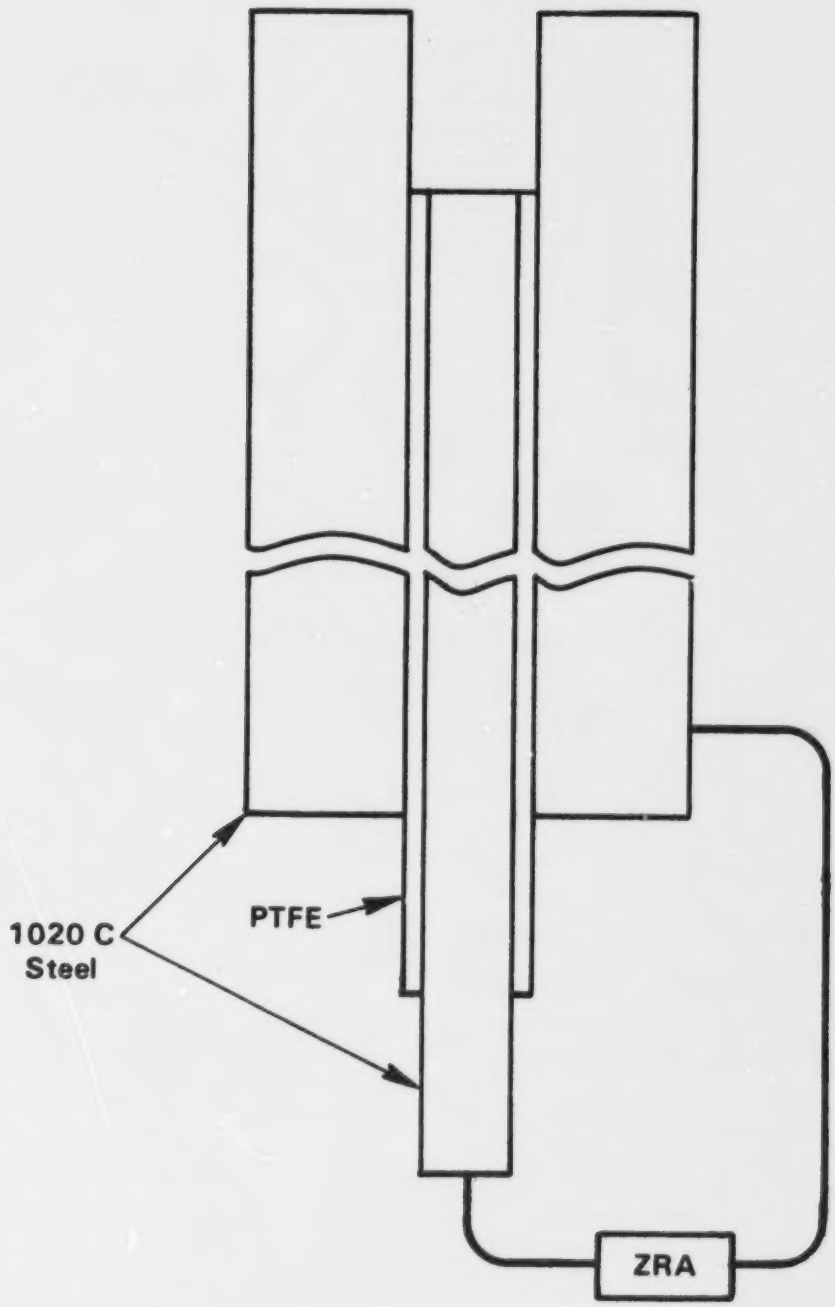

ZRA = Zero Resistance Ammeter

Figure 3.11. Schematic of pit-propagation monitor.

BEST COPY AVAILABLE

anodic currents flowing from the pits. The pitting currents were monitored during the next five days. For the Fe_3O_4 pits, the current densities fluctuated between 5.1 and 11.6 $\mu A/cm^2$. (2.17 $\mu A/cm^2$ is equal to 1 mil/yr for iron). Thus, the pitting rates were quite low. Pitting current densities for the glass-plugged pits were even lower, varying between 0.51 and 1.2 $\mu A/cm^2$ over the five-day period.

Because of the low pitting rates observed, it was decided to attempt to stimulate the pits by anodically polarizing them. The specimens were galvanostated at 15 mA/cm^2 for 24 hours. For the Fe_3O_4 pit, approximately 400 mV of polarization was required to achieve the desired current. On the other hand, over 5 V of polarization was required to achieve the same current density for the frit-plugged pit, suggesting that there were high potential drops across the frit.

After the polarization, the pitting currents were again measured and found to be cathodic. Over a period of two days the current densities remained cathodic, at values ranging between ≤ 1 $\mu A/cm^2$ and 72.5 $\mu A/cm^2$ for the Fe_3O_4 pit and between 11 and 18 $\mu A/cm^2$ for the frit-plugged pit.

It was concluded from the experiments that Fe_3O_4 packing of the pit was the better method of occluding the pit, of the two techniques which were studied. It also appeared from this experiment that anodic stimulation was detrimental to pit initiation since cathodic currents were measured afterwards. However, the zero-resistance ammeter was connected between the pit and bulk surface immediately following anodic stimulation. This produced cathodic currents, since the anodic stimulation made the pit more noble than the boldly exposed surface. The cathodic currents produced an increase in pH within the pit, altering the pit environment. Different results might have been obtained if the pit had remained uncoupled after anodic stimulation and the potential permitted to depolarize prior to coupling.

In a second experiment, both cells were set up with aspect ratios of 3:1, and the pits were packed with an Fe_3O_4 slurry. For the first 24 hours, nitrogen was bubbled through both cells; one cell (cell A) was left uncoupled, whereas in the other (cell B) the pit was anodically stimulated at 15 $\mu A/cm^2$. After 24 hours, cell B was disconnected from the galvanostat, oxygen flow was started in both cells, and the potential differences between the pit and the boldly exposed surfaces were measured for both cells. For cell A, the pit was 15 mV negative to the boldly exposed surface, whereas for cell B, the pit was 20 mV positive (noble) to the boldly exposed surface. Over the next 24 hours, the pit in cell B maintained a noble potential of 15 to 20 mV with respect to the boldly exposed surface and accordingly, the experiment was terminated. From this experiment, it was confirmed that anodic stimulation of the pit was not beneficial to pit initiation.

Following the potential measurement on cell A, the pit and the boldly exposed surface were coupled through a zero-resistance ammeter and the current was monitored as a function of exposure time. During the first

BEST COPY AVAILABLE

50 minutes, the current density increased from 43 $\mu A/cm^2$ to about 180 $\mu A/cm^2$ and then decreased over the next 1400 minutes, and actually went negative after 1125 minutes, indicating protection of the pit. Pitting reinitiated after about 1450 minutes of exposure, and current density increased over the next 2800 minutes to about 65 $\mu A/cm^2$. The current density then fluctuated over the next 1200 minutes between 65 and about 3 $\mu A/cm^2$.

These current fluctuations may have been the result of inadequate control of oxygen flow and temperature within the cell or may be inherent in the pitting process on carbon steel. For example, the growth and spalling of oxide films on the boldly exposed surface may produce sizable fluctuations in pitting currents if the rate of pitting is controlled by the cathodic reaction. To test the sensitivity of the pitting current to temperature and oxygen flow rate, these parameters were varied briefly during the course of the test. A 10 C drop in the temperature reduced the pitting current density from 16.7 $\mu A/cm^2$ to 7.2 $\mu A/cm^2$. Varying the oxygen flow rate had a similar affect, with the current density increasing with increasing oxygen flow rate.

Based on the observed dependence of the pitting current on the oxygen flow rate, it was concluded that the rate of pitting is controlled, to some extent, by the kinetics of the reduction reaction. To test this hypothesis, the pit was disconnected from the boldly exposed carbon-steel surface and connected to a platinum counter electrode; the current density immediately increased several orders of magnitude to about 3.26×10^3 $\mu A/cm^2$ but did decay over the next 700 minutes to about 1.09×10^3 $\mu A/cm^2$, a value which is nevertheless considerably higher than values measured for the standard pit geometry. These high currents measured with the latter geometry and the decay in the currents may be associated with a diffusion-limited pitting rate.

Because of the problems encountered with temperature and oxygen control, the pit cell was redesigned. The TEFLON cell body was replaced with a double walled PYREX* cell body. With the new design, the cell is heated by flowing heat transfer fluid between the inner and outer cell walls; the heat transfer rate is much greater than in the previous design and thus the cell temperature is not a function of the oxygen flow rate.

3.2 Hydrogen Embrittlement

Hydrogen-embrittlement studies are being conducted to determine the potential for failure of the waste container as a result of degradation of its mechanical properties by hydrogen. Anticipated sources of hydrogen are corrosion and radiolytic reactions. During the past quarter, experiments were conducted to evaluate the effects of hydrogen on the properties of iron. The iron was provided by Armco, Incorporated, in the form of 1 x 3 x 7-inch ingots, which were described in

---

*PYREX is registered trademark of Corning Glass Works.

the previous quarterly report.[3.3] It is anticipated that relatively pure iron may be proposed as a candidate overpack corrosion-allowance material.

3.2.1 Fracture-Toughness Tests

Fracture-toughness experiments were performed with compact-tension fracture-mechanics specimens that were machined from the ingots as cast. Parallel experiments were conducted in 1000 psi (6.9 MPa) nitrogen and in 1000 psi (6.9 MPa) hydrogen to provide a relative indication of the degree of degradation of the resistance of the material to cracking. The experiments were intended to be standard elastic-plastic fracture-toughness experiments conducted in general accordance with ASTM Standard E813. However, as discussed in the following section, the behavior of the iron specimens was such that neither elastic-plastic nor linear-elastic (per ASTM Standard E399) standard fracture-toughness-measurement procedures could be followed.

The elastic-plastic fracture-toughness, or J-integral, experiment provides a measure of the work required to initiate and drive a crack through a ductile metal. By applying a constant, slow, crack-opening-displacement rate to the specimen and monitoring the load on the specimen and the crack length continuously, the energy release rate per unit crack advance, which is equal to the J-integral, can be estimated. The plot of J-integral versus change in crack length is known as the J-resistance curve, which contains information regarding the material's resistance to cracking. Comparison between the material's J-resistance curve and the applied J-integral in service, resulting from the stress state in the container wall and the presence of a flaw, should allow calculation of the critical flaw size which the container can support and thereby contribute to failure criteria for estimation of containment life. The intersection of the J-resistance curve with the blunting line, which is a mathematically derived estimate of the extent of apparent, artificial crack growth that results from crack-tip blunting, defines the elastic-plastic fracture toughness or resistance to crack initiation, J_{IC}. The resistance to subsequent steady ductile crack growth is given by the tearing resistance, which is the slope of the J-resistance curve, or by the tearing modulus, which is a nondimensional quantity that is proportional to the tearing resistance. The fracture toughness and the tearing resistance or tearing modulus are frequently used measures of resistance to ductile fracture.

3.2.2 Results and Discussion

Figure 3.12 presents approximate J-resistance curves that were generated from the fracture-toughness-experiment data. There was some uncertainty in determining the actual crack lengths, for reasons discussed later in this section.

BEST COPY AVAILABLE

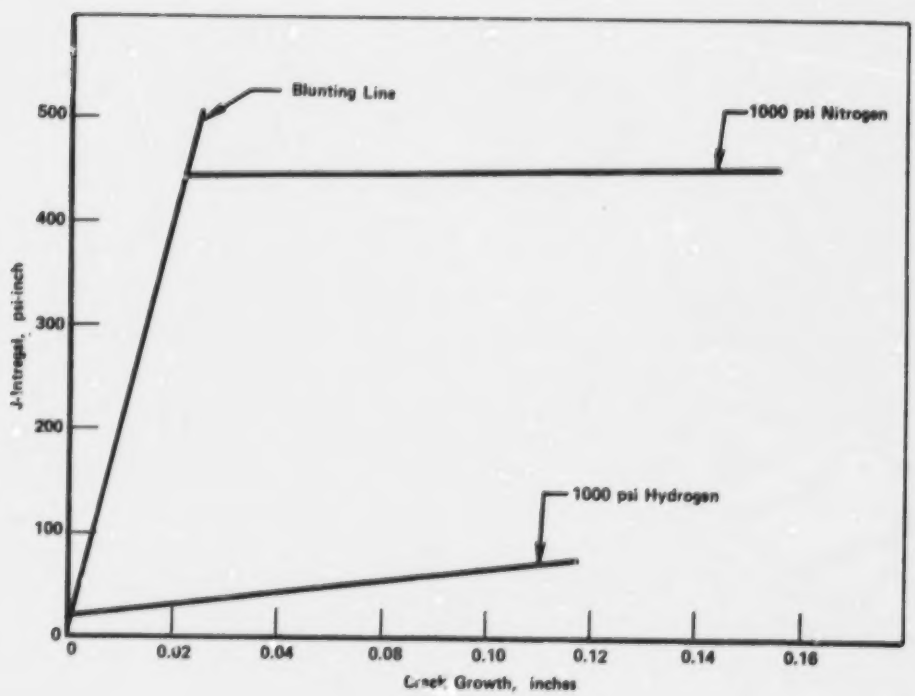

Figure 3.12. J-resistance curves for iron specimens.

BEST COPY AVAILABLE

The J-resistance curves indicate very low toughness in both the nitrogen (reference) and hydrogen environments, with values of J_{IC} equal to approximately 440 psi-inch and 20 psi-inch, respectively. As with many other materials, such as the cast steels that have been reported on previously, hydrogen reduced the resistance to initiation of a ductile crack. The tearing-resistance values also are extremely low and a greater amount of rapid crack growth was observed in both environments than had been anticipated.

These results suggest that fracture proceeded in an elastic or brittle manner, with little or no plastic deformation preceding crack initiation. In essence, this is what occurred in the experiments, except that there was significant ductility prior to crack initiation--sufficient to rule out standard linear-elastic quantification of the fracture behavior. Continuous monitoring of crack length during the fracture-toughness experiments, using a direct-current electric-potential-drop method, provided an indication of the manner in which cracking occurred in this environment. In the nitrogen environment, the specimen was loaded elastically at first, and then plastic deformation at the crack tip occurred as the specimen was loaded further. Following what appeared to be a significant amount of plastic deformation, such that standard linear-elastic measures of fracture toughness such as K_{IC} could not be determined with validity, a sudden drop in load was detected. This load drop was accompanied by a sudden rise in the signal from the electric-potential-drop probes, indicating a rapid increase in crack length. This "pop-in" form of crack initiation sometimes is observed in brittle, high-strength materials, but typically it is not preceded by any appreciable deformation. Thus, standard test methods could not be applied to interpretation of the results of these experiments.

However, some comparisons may be made between the cracking behavior in the nitrogen and hydrogen environments. Crack growth in the hydrogen environment proceeded in a manner similar to that described above for crack growth in the nitrogen, except that pop-in crack initiation was preceded by a small amount of steady, possibly ductile, crack growth. This evidently is reflected in the J-resistance curves, which indicate that hydrogen promoted a large reduction in resistance to crack initiation. However, because of the rapid nature of the subsequent pop-in cracking, the precise crack length indicated by the electric-potential-drop probes at a given point in an experiment was uncertain with the calibration procedure used. Thus, the J-resistance curves in Figure 3.12 are only approximate, and the extent of cracking in the hydrogen environment prior to pop-in is not known precisely.

The results presented above indicate that the iron samples being studied may be subject to rapid cracking, independent of environment. However, the presence of a hydrogen environment promoted steady cracking prior to pop-in. This behavior may indicate a sensitivity of this material to

sustained-load subcritical-crack growth. Hydrogen evolved in a repository could promote ductile crack initiation and growth of flaws in a container in which local stress-intensity factors are too low to promote pop-in cracking, and a subcritical flaw thus could grow to critical size and cause failure of the container. Further study may be needed to determine whether this is likely to be the case and whether sensitivity to hydrogen degradation may be mitigated by suitable heat treatment.

3.2.3 Future Work

During the next quarter, hydrogen-embrittlement experiments are planned with welded cast-steel samples that are to be provided by Manufacturing Sciences Corporation, another NRC contractor. The objective will be to determine whether the heat-affected zone becomes sensitive to hydrogen embrittlement. If difficulties in obtaining these materials are encountered, further studies of the iron castings from Armco will be performed in the interim to determine whether this material is susceptible to subcritical-crack growth and to identify the causes and possible remedies for such sensitivity.

3.3 Corrosion Correlations

The objective of the corrosion-modeling effort is to provide information about corrosion processes that affect the waste-container materials in a repository environment. Models under development deal with general corrosion and pitting.

During this quarter, efforts on the general-corrosion correlation focused on incorporating a finite rate of film growth into the model (that is, relaxing the assumption that film growth at the surface is so rapid that the rate of supply of oxidizing species to the surface is not altered). This change in the model will ultimately permit a quantitative assessment of the relative importance of diffusion in the solution and growth of the oxide film.

The pitting-corrosion correlation was examined in light of the results of the recently completed experimental studies of pit growth. Because the experiments indicated that the pitting current is significant, the treatment of pitting current in the pitting-corrosion model was analyzed to assess its dependence on other parameters.

3.3.1 General Corrosion

Analyses of general corrosion that have been carried out in this program to date have been based on the so-called "maximum-rate model", in which transport of the oxidizing species within the solution to the container surface is assumed to be the rate-controlling process for oxidation. In other words, the kinetics of film growth at the surface is assumed to take place very rapidly by comparison and thus not to affect in any way the rate of supply of the oxidizing species to the surface. This condition is expressed mathematically as $C_i(r_o,t) = 0$, where C_i is the

concentration of the ith oxidizing species, r_o is the container radius, and t is time.

During the past quarter efforts have been undertaken to relax the assumption of maximum-rate kinetics and include a model of film growth at the metal surface that accounts for the finite rates of mass transport across the film thickness. The film-growth model being used is that developed by Chao, Lin, and Macdonald[3.4] for growth of a coherent oxide film and is expressed as

$$\frac{dL}{dt} = \frac{A(B-1)}{\exp(2KL)-1} \quad , \tag{3.1}$$

where $K \equiv F\varepsilon/(RT)$, with F being the Faraday constant, R the gas constant, T the absolute temperature, and ε the electric field inside the film (a constant, about 10^6 V/cm, directed along the thickness). In Equation 3.1, dL/dt is the rate of oxide penetration into the container and A and B are parameters which depend upon the redox potential at the container/solution interface.

The coupling of the film-growth model to the model of mass transport through the solution occurs through the parameters A and B, both of which are dependent upon such factors as the solution pH and the concentrations of oxidizing and reducing species at the film/solution interface. Moreover, dL/dt must also be directly related to the rate of supply of the oxidizing species to the film surface, i.e.,

$$\frac{dL}{dt} = \frac{M}{\rho X} D \frac{\partial C}{\partial r}(r_o,t) \quad , \tag{3.2}$$

where M and ρ are the molecular weight and density, respectively, of the metal, X the reaction stoichiometry, and D and C the diffusivity and concentration, respectively, of the oxide species in the solution. Of course, if more than one oxidizing species is present in the solution, then the right-hand side of Equation 3.2 would involve a summation involving the contribution of each to dL/dt.

The approach being taken in including film-growth kinetics in the anaysis of general corrosion is essentially one in which self-consistency is sought. Basically, at any given instant of time in the calculation, an iterative approach is used to adjust the concentrations of species at the film/solution interface until the rates of film growth, as predicted by Equations 3.1 and 3.2, are equal. This, of course, is considerably more complicated than the simple maximum-rate kinetics which have been used previously. However, the resultant model will represent situations much more realistically.

Initial applications of this approach will be directed to very simple models, e.g., one chemical species in the solution, that being a radiolytically produced oxidizing species, nominally O_2. This particular

problem had been considered in detail previously[3.5] on the basis of the more elementary maximum-rate kinetics. Even this simple model will provide some quantitative understanding of the interrelationships between film-growth kinetics and radiolytic production of the oxidizing species. In addition, the relative importance of the two basic mass-transport processes, namely diffusion in the solution and growth of the oxide film, can be quantitatively assessed.

3.3.2 Pitting Corrosion

In Battelle's most recent annual report[3.6] on this program, a pit-growth model was developed based on the well-known transport theory characterizing a dilute solution of a "binary electrolyte", i.e., a solution containing one cation species and one anion species. (The general theory of binary electrolytes has been presented in detail by Newman[3.7].) Ionic transport by both chemical diffusion and electro-migration were included. Pit growth was assumed to occur as a result of anodic dissolution of the metal, the dissolved metal taken as the cation species in the solution.

The principal goal of our original analysis was to predict the time-dependence associated with pit growth. However, the experimental studies of pit growth, reported in Section 3.1.3, have demonstrated a strong sensitivity of pitting current to certain experimental conditions. In this light, attention was directed during the past quarter to an analysis of the pitting current, as predicted in the basis of the binary-electrolyte model, to assess its dependence on pertinent experimental parameters. The results are summarized below, using nomenclature that is consistent with that used in Reference 3.6.

Recalling that the pit model involves a cylindrical pit, with ionic transport taking place one-dimensionally along the length of the pit, the total current, i, associated with growth of a single pit is given by

$$i = F\,(z_+N_+ + z_-N_-) \quad , \tag{3.3}$$

where F is the Faraday constant, z_+ and z_- are the respective numbers of proton charges associated with the cation and anion, and N_+ and N_- are the respective fluxes of cations and anions along the pit length. Since the anion does not undergo chemical reaction at the pit base, and since it is assumed that no homogeneous chemical reactions take place within the solution, it follows that $N_- = 0$ everywhere inside the pit, in which case Equation 3.3 reduces to

$$i = Fz_+N_+ \tag{3.4}$$

From Equation 3.25 of Reference 3.6, it follows that

$$N_+ = -D_+\left(\left|\frac{z_+}{z_-}\right| + 1\right)\frac{c_+(h) - c_+(0)}{h}, \tag{3.5}$$

where D_+ is the cation diffusion coefficient, and $c_+(0)$ and $c_+(h)$ are the respective cation concentrations in the solution at the pit mouth and pit base, with h being the instantaneous pit depth. (The sign convention used in the development of this model is such that $N_+ < 0$ implies cation flow away from the pit base.) Moreover, from Equation 3.23 of Reference 3.5, one can show that

$$c_+(h) = c_+(0)\exp\left(\frac{z_-F}{RT}\left[\phi(0) - \phi(h)\right]\right), \tag{3.6}$$

where R is the gas constant, T the absolute temperature, and where $\phi(0)$ and $\phi(h)$ are the respective electrostatic potentials at the pit mouth and pit base.

Combining Equations 3.4 to 3.6,

$$i = Fz_+D_+\left(\left|\frac{z_+}{z_-}\right| + 1\right)\frac{c_+(0)}{h}\left\{1 - \exp\left[\frac{z_-F}{RT}\left(\left[\phi(0)-\phi(h)\right]\right)\right]\right\}. \tag{3.7}$$

Clearly, Equation 3.7 constitutes a relationship between the pitting current and the potential difference across the pit length. One limiting case which is of particular interest is that for which $c_+(h) >> c_+(0)$, which corresponds to the assumption that the concentration of dissolved metal immediately adjacent to the base of the pit far exceeds that at the pit mouth, which is adjacent to the bulk solution. For this special case, Equation 3.7 becomes

$$i \cong -Fz_+D_+\left(\left|\frac{z_+}{z_-}\right| + 1\right)\frac{c_+(0)}{h}\exp\left(\frac{z_-F}{RT}\left[\phi(0) - \phi(h)\right]\right). \tag{3.8}$$

Equation 3.8 can be equivalently expressed in the alternative, and somewhat more familiar, form

$$\phi(0) = \phi(h) + \frac{RT}{|z_-|F}\ln\left(\frac{i}{i_o}\right), \tag{3.9}$$

where the minus sign on the right-hand side of Equation 3.8 has been dropped, and where

BEST COPY AVAILABLE

$$i_o \equiv Fz_+D_+\left(\left|\frac{z_+}{z_-}\right| + 1\right)\frac{c_+(0)}{h} \quad . \qquad (3.10)$$

It is clear, from either Equation 3.8 or 3.9, that the pitting current is indeed sensitive to a number of parameters. For instance, assuming the h^{-1} factor on the right-hand side of Equation 3.8 is the only factor therein that actually varies with h, it follows that i varies as h^{-1}, and therefore the pitting current decreases as the pit becomes deeper. Likewise, if experimental conditions cause a variation of the potential at the crevice mouth, $\phi(0)$, the relative effect on i would be substantially greater because of the exponenential dependence of i upon $\phi(0)$. Such an effect may, in fact, be related to the relatively high pitting currents that were measured in Battelle experiments involving the use of a platinum counter electrode (see Section 3.1.3 of this report).

The studies of pitting corrosion will continue into the next quarter. For example, effects of variations of the pit-depth distribution on the overall pitting current will be considered. In addition, introductory calcuations of possible effects of radiolytic production of chemical species on the pit-growth rate will be carried out.

3.4 References for Section 3

(3.1) D. Stahl and N. E. Miller (Compilers), "Long-Term Performance of Materials Used for High-Level Waste Packaging", Annual Report, Year Two, NUREG/CR-3427, BMI-2113, Vol. 4 (June 1984), pp. 3-67 ff.

(3.2) M. B. Strauss and M. C. Bloom, "Cracking of Low Carbon Steel by Ferric Chloride Solutions", Corrosion, Vol. 16, No. 11, 1960, p. 109.

(3.3) "Long-Term Performance of Materials Used for High-Level Waste Packaging", D. Stahl and N. E. Miller (Compilers), NUREG/CR-3900, Vol. 2 (January 1985), pp. 3-32 ff.

(3.4) C. Y. Chao, L. F. Lin, and D. D. Macdonald, "A Point Defect Model for Anodic Passive Films", J. Electrochem, Soc., 128 (1981), 1187.

(3.5) "Long-Term Performance of Materials Used for High-Level Waste Packaging", D. Stahl and N. E. Miller (Compilers), Annual Report, Year Two, NUREG/CR-3427, BMI-2113, Vol. 4 (June 1984), pp. 3-114 ff.

(3.6) "Long-Term Performance of Materials Used for High-Level Waste Packaging", D. Stahl and N. E. Miller (Compilers), Annual Report, Year Two, NUREG/CR-3427, BMI-2113, Vol. 4 (June 1984), pp. 3-126 ff.

(3.7) J. S. Newman, Electrochemical Systems, Prentice-Hall, Inc. (Englewood Cliffs, N. J., 1973), pp. 223 ff.

BEST COPY AVAILABLE

4. INTEGRATED SYSTEM PERFORMANCE

The purpose of the system-performance task is to obtain a better understanding of the phenomena which affect the long-term performance of waste packages at the system level. Knowledge gained in these studies will aid in assessing the adequacy of system-performance models for nuclear waste packages.

During the past quarter, emphasis has been placed on water-chemistry studies, groundwater-radiolysis studies, and integral experiments.

The water-chemistry studies will improve our understanding of the water chemistry in the vicinity of the waste package. This will provide information on how the corrosion of the metallic barriers and the leaching or dissolution of the waste form alter, and are altered by, the local water chemistry. The water-chemistry studies will also provide information on the chemical speciation of radionuclides released from the waste form. This information will be useful for assessing the transport rate of these radionuclides through the waste package. Efforts in water-chemistry studies during this quarter focused on the waste form, and the results are discussed in Section 2.4 of this report.

The groundwater-radiolysis studies will provide information on the concentrations of radiolytic species in the vicinity of the waste package. These species can affect the corrosion of the metallic barriers and the chemical speciation of the radionuclides released from the waste form. Such phenomena can influence the expected period of absolute containment for a waste package, as well as the release rate of radionuclides from the waste package to the repository environment after breach of containment.

The integral experiments are being assembled to provide information on what combined effects are important in the long-term performance of nuclear waste packages. These experiments will provide an approximate simulation of the environment which a waste package and its components will see during their lifetime. These experiments will also provide some information on the rates of releases and cumulative releases of radionuclides from high-level waste glass and spent-fuel waste forms for a variety of simulated-waste-package failures.

4.1 Groundwater-Radiolysis Studies

Radiolysis of groundwater near the waste package can alter the local water chemistry and thus affect the long-term performance of waste packages. Effects on the local water chemistry can include changes in pH and oxygen potential, as well as the production of additional species which may have a deleterious effect on the waste-package materials. As reported previously, other investigators have observed that gamma radiation may have adverse effects on the time-to-failure performance measure for metal components which are exposed to water[4.1].

The objective of these studies is to develop a generalized model for analyzing the radiolysis of unaltered groundwater systems and the radiolysis of groundwater systems whose composition has been altered by the presence of other materials such as packing and corrosion products. The model will provide information on the expected concentrations of radiolysis products in the vicinity of the metallic components of the waste package; this information will be used in the canister-materials task of the program. The model will also provide a means of assessing the abbreviated groundwater-radiolysis model which is part of the general-corrosion model described in Section 3.3.1. The model will also provide a vehicle for determining effective rate constants for reactions included in the water-radiolysis component of the corrosion model.

The approach taken in these studies is to develop and benchmark a description of the radiolysis of pure water which might contain hydrogen and/or oxygen. The current description is being extended to account for the presence of anions and cations which may be present in significant amounts in groundwaters of interest. As the description of groundwater radiolysis is developed, it is being benchmarked against experimental data available from the literature. As part of this effort, gamma-energy deposition calculations were performed to determine energy deposition rates to groundwater and to the materials surrounding spent-fuel and commercial high-level waste packages. Results of these energy-deposition calculations were reported previously, and several mechanisms for the radiolysis of water were evaluated on the basis of their ability to predict the behavior of water-radiolysis experiments described in the literature.[4.1] Of these, the mechanism presented by Rosinger and Dixon[4.2] was chosen as a basis mechanism upon which a generalized description for groundwater radiolysis would be developed.

Work during this past quarter has been directed toward comparing the effects of G-values on the calculated results. (The G-value indicates the source rate to solution for a given aqueous species.) This comparison has been performed for a simulation of the radiolysis of water containing hydrogen and oxygen for seven sets of G-values used by other investigators and a set used in the calculations reported previously[4.3].

4.1.1 Effects of G-Value Sets On Calculated Concentrations

The G-values used and reported by other investigators are shown in Table 4.1, along with the set which was used in our previously-reported calculations[4.3]. On an order-of-magnitude basis, there is little variation between respective values shown in Table 4.1 (for those which are reported), with the variation from lowest value to highest generally less than 50 percent. Each of these sets of values was used in a water-radiolysis simulation where the initial dissolved hydrogen and oxygen concentrations were 7.33×10^{-4} and 7.5×10^{-5} m/liter, respectively, with a gamma dose rate of 9.22×10^{18} eV/l-sec. Table 4.2 shows values calculated at 1×10^{4} seconds for the pH, K_w, and H_2O_2, H_2, and O_2

Table 4.1. G-values used by various investigators for related systems.

Species	G-Values					
	Ref. 4.3 (BCL)	Ref. 4.4	Ref. 4.5	Ref. 4.6	Ref. 4.7	Ref. 4.8
e^-	2.8	2.8	2.7	2.7	2.7	2.8
H^+	2.9	2.9	2.8		2.7	2.9
OH^-	.1	.1	.1			.1
OH	2.7	2.7	2.75	2.7	2.86	2.8
H	.48	.44	.55	.6	.61	.55
H_2	.45	.45	.45	.45	.43	.45
H_2O_2	.7	.72	.7	.75	.61	.7
HO_2	.02				.03	
H_2O	-4.25	-7.04	-4.25		-4.14	-4.3*

*Calculated from the values reported.

Table 4.2. Calculated concentrations, pH, and K_w for a water-radiolysis simulation using various sets of G-values.

Source of G-Values	Values, Calculated at 10^4 sec				
	pH	K_w	$[H_2O_2]$ (m/l)	$[H_2]$ (m/l)	$[O_2]$ (m/l)
Ref. 4.3 (BCL)	6.9	1.02×10^{-14}	6.94×10^{-8}	5.96×10^{-4}	4.82×10^{-14}
Ref. 4.4	6.9	1.01×10^{-14}	6.94×10^{-8}	5.81×10^{-4}	9.67×10^{-16}
Ref. 4.5	6.9	1.01×10^{-14}	6.90×10^{-8}	5.81×10^{-4}	9.69×10^{-16}
Ref. 4.6	11.6	1.01×10^{-14}	8.54×10^{-10}	5.81×10^{-4}	5.29×10^{-16}
Ref. 4.7	6.9	1.02×10^{-14}	6.22×10^{-8}	5.81×10^{-4}	7.33×10^{-14}
Ref. 4.8	6.9	1.01×10^{-14}	6.68×10^{-8}	6.19×10^{-4}	8.34×10^{-16}

concentrations. Each set of G-values leads to the same pH prediction except for that of Reference 4.6, which is of limited applicability to this system since those values are for brine solutions. In this table, the ion product for water is not significantly affected by variations in G-values. Agreement is also within about 10 percent for the H_2O_2 concentrations, except for those of Reference 4.6, where there is a difference of about two orders of magnitude. The variation in calculated H_2 concentrations is less than 10 percent for all of the G-value sets in Table 4.2. The O_2 concentrations, however, vary over a range of two orders of magnitude for the G-values used. Data in Table 4.2 show that the calculated O_2 concentrations can be sensitive to G-values since even small variations, such as between those of Reference 4.8 and the BCL values, can cause a two-order-of-magnitude change in the calculated O_2 concentration. Here the percentage changes in e^-, H^+, OH^-, OH, H, H_2, and H_2O_2 G-values are 0, 0, 0, 3.7, 14.6, 0, and 0. The difference between 0 and 0.02 for the HO_2 G-value cannot in itself cause the change, since the BCL value of 0.02 stands between the values used in References 4.7 and 4.8, namely 0 and 0.03. A similar observation can be applied to the G-value for H when compared to those of Reference 4.4. The sensitivity of the calculated O_2 concentrations to G-values is thus a factor which should be considered when performing predictive calculations.

4.1.2 Generation of G-Values to Correlate with Benchmark Data

To examine whether small changes in G-values can improve the ability of the radiolysis model to predict benchmark data described in an earlier report[4.1], the G-values were varied slightly without regard to their reported variation with factors such as pH and ionic strength[4.9]. Mass balance constraints were, however, applied. The benchmark data[4.10] were obtained for a water-radiolysis simulation with initial H_2 and O_2 concentrations of 7.33×10^{-4} and 7.6×10^{-5} m/liter and a dose rate of 9.22×10^{18} eV/l-sec. For agreement with these data, the H_2O_2 concentration should be approximately 2.8×10^{-4} m/liter at approximately 4×10^{3} seconds. Agreement was not observed for this particular case using the current reaction set and rate constants for this case. Studies have shown that the system can be relatively insensitive to changes in the rate constants[4.5]. Effects of small changes in G-values were therefore examined.

Two sets of G-values, designated A and B, are shown in Table 4.3. The values shown here are similar in magnitude to those shown in Table 4.1 and were used in a simulation using the same conditions as were used for the data shown in Table 4.2. The results of calculations using sets A and B, which are shown in Table 4.4, differ by four orders of magnitude from results shown in Table 4.2 for the predicted H_2O_2 concentrations. The H_2O_2 concentrations calculated with G-value sets A and B are close to the desired result, namely about 3×10^{-4} m/liter. At 1000 seconds, however, the calculated H_2O_2 concentration does briefly drop to a level similar to those shown in Table 4.2. Understanding of this phenomenon

Table 4.3 G-value sets generated to improve agreement with benchmark data.

Species	G-Value Sets A	B
e^-	1.8	1.8
H^+	2.7	3.1
OH^-	.1	.1
OH	2.7	2.86
H	.55	.44
H_2	.45	.43
H_2O_2	.7	.845
HO_2	.02	.02
H_2O	-4.2	-4.7

Table 4.4 Calculated concentrations, pH, and K_w for a water-radiolysis simulation using G-values chosen to improve agreement with benchmark data.

G-Value Set	Values, Calculated at 10^4 sec pH	K_w	$[H_2O_2]$ (m/l)	$[H_2]$ (m/l)	$[O_2]$ (m/l)
A	2.9	2.30×10^{-14}	1.30×10^{-4}	3.26×10^{-5}	8.93×10^{-6}
B	2.7	2.11×10^{-14}	4.19×10^{-4}	7.01×10^{-5}	1.13×10^{-4}

60.

BEST COPY AVAILABLE

is encumbered by the complexity associated with the availability of several reaction pathways for each reactive species in the mechanism.

4.1.3 Conclusions

A 55-reaction mechanism[4.2] for the radiolysis of water was used to examine the sensitivity of calculated results to the G-values assumed for the system. The sets of G-values used were similar in magnitude to each other. It was found that the calculated O_2 concentration may be particularly sensitive to small variations in G-values. Other calculations show that free variation of the G-values, within conservation-of-mass constraints, can cause significant variation in the response of the model.

4.2 Integral Experiments

Combined effects are often targeted for detailed study on the basis of engineering judgment. However, in formulating a system description or assessing licensing applications, there must be some basis for ensuring that important combined-effects processes are not overlooked. There is thus a need to perform a test to provide investigators with a reasonably realistic view of the processes that may contribute to waste-package degradation. Such a test may help confirm the importance of some processes already believed to be important, and may also identify others not previously considered. The result will be the establishment of a technical basis for, and identification of the level of detail necessary in, a system model and a licensing application.

The primary purpose of the integral experiments is to provide scoping information that will help identify potentially important combined effects. The secondary purpose of these experiments is to provide qualitative information on corrosion phenomena, release rates, and water chemistry for spent-fuel and commercial high-level waste packages.

4.2.1 Status

All major components of the apparatus have arrived from vendors. Construction of the 30 test chambers has been completed, as well as the support assembly which will hold the test chambers in place in the oven. The space in the hot cell and in the cold-operations area has been allocated. The gas purge fittings have been mounted on the simulated groundwater source drums, and the test chambers have been mounted on the support assembly. Testing of the dissolved-oxygen meter is under way.

A sample of high-level-waste glass ATM-5 (commercial waste vitrified in PNL 76-68 glass) has been received from Battelle's Pacific Northwest Laboratories. Detailed characterization of this glass will be carried out by Pacific Northwest.

4.2.2 Future Work

Construction of the apparatus will continue in the near term. Concurrent with this activity, specimen preparation will be initiated and necessary ancillary materials such as rock, simulated corrosion products, and corrosion specimens will be prepared. Spent-fuel samples will also be sectioned, capped, and "prefailed".

4.3 References for Section 4

(4.1) "Long-Term Performance of Materials Used for High-Level Waste Packaging", D. Stahl and N. E. Miller (Compilers), NUREG/CR-3427, Vol. 4, BMI-2113 (June 1984), Section 4.

(4.2) E.L.J. Rosinger and R. S. Dixon, "Mathematical Modeling of Water Radiolysis: A Discussion of Versions", AECL-5958 (1977).

(4.3) "Long-Term Performance of Materials Used for High-Level Waste Packaging", D. Stahl and N. E. Miller (Compilers), NUREG/CR-3900, Vol. 2, (January 1985), Section 4.

(4.4) H. Christensen and E. Bjergbakke, "Radiolysis of Groundwater from HLW Stored in Copper Canisters", Materials Research Society Symposia Proceedings, Vol. 15, Scientific Basis for Nuclear Waste Management, pp. 429-36 (1983).

(4.5) A. W. Boyd, M. B. Carver, and R. S. Dixon, "Computed and Experimental Product Concentrations in the Radiolysis of Water", Rad. Phys. Chem., 15, 177-85 (1980).

(4.6) G. H. Jenks, "Review of Information on the Radiation Chemistry of Materials Around Waste Canisters in Salt and Assessment of the Need for Additional Experimental Information", ORNL-5607 (March 1980).

(4.7) W. G. Burns, et al, "Effects of Radiation on the Leach Rates of Vitrified Radioactive Waste", J. Nucl. Mat., 107, 145-70 (1982).

(4.8) L. M. Dorfman and G. E. Adams, "Reactivity of the Hydroxyl Radical in Aqueous Solutions", COM-73-50623, p. 4 (June 1973).

(4.9) I. G. Draganic and Z. D. Draganic, The Radiation Chemistry of Water, Academic Press, New York (1971).

(4.10) C. J. Hochanadel, "The Radiation-Induced Reaction of Hydrogen and Oxygen in Water at 25 to 250 C", Proc. Intl. Conf. Peaceful Uses of Atomic Energy, United Nations, 7, pp. 521-25, (1955).

BEST COPY AVAILABLE

5. QUALITY ASSURANCE

Quality assurance surveillance of the various program activities continues. No procedures were prepared or revised during this quarter. As of this date there are 34 approved QA procedures and two approved work instructions for the program.

A summary of the procedures which are being used to conduct the experimental program is given in Table 5.1. Included is the procedure number, the current revision number, the title, and the status.

Quality assurance surveillance activities will continue. Procedures will be revised and new ones prepared as necessary to meet program requirements.

Table 5.1. Status of NRC waste packaging program QA procedures.

Procedure No.	Title	Status
WF-PP-1 Revision 0	Procedures for Record Keeping and Documentation for NRC Waste Form System Model Development	Approved
WF-PP-5 Revision 0	Procedures for Record Keeping and Documentation for Separate Effects Model Development	Approved
WF-PP-10 Revision 0	Laboratory Procedure for Preparation of Glasses for NRC Waste Form Project	Approved
WF-PP-11 Revision 1	Laboratory Procedures for Preparation of Teflon-Leach Containers	Approved
WF-PP-14 Revision 1	Laboratory Procedure for Leaching Glass Samples	Approved
WF-PP-16 Revision 0	Laboratory Procedure for Operating the Orton Dilatometer	Approved
WF-PP-20 Revision 0	Procedure for Determining the Corrosion Rates of Alloys at High Temperatures	Approved
WF-PP-25 Revision 0	Procedure for Preparation of Carbon-Steel Casting	Approved
WF-PP-26 Revision 0	Procedure for Preparation of Steel Hydrogen-Embrittlement Test Specimens	Approved
WF-PP-26.1 Revision 0	Procedure for Preparation of Hydrogen-Embrittlement Test Specimens from Steel or Iron Samples	Approved

Table 5.1. Continued.

Procedure No.	Title	Status
WF-PP-27 Revision 4	Procedure for J-Testing Compact Tension Specimens	Approved
WF-PP-28 Revision 1	Procedure for Performing Tension Tests of Steel Specimens	Approved
WF-PP-29 Revision 0	Procedure for Conducting Hydrogen-Absorption Experiments	Approved
WF-PP-30 Revision 0	Laboratory Procedure for Preparation, Cleaning, and Evaluation of Titanium Grade-12 Specimens for Corrosion Studies of the Overpack Performance for the NRC Waste Packaging Program	Approved
WF-PP-31 Revision 0	Laboratory Procedure for Preparation, Cleaning, and Evaluation of Cast and Wrought Carbon Steel Specimens for Corrosion Studies of the Overpack Performance for the NRC Waste Packaging Program	Approved
WF-PP-32 Revision 0	Procedure for Preparation of Brine A for Corrosion Testing Under Simulated Repository Conditions	Approved
WF-PP-33 Revision 0	Procedure for Preparation of Simulated Basalt Groundwater Solution	Approved
WF-PP-33.1 Revision 0	Procedure for Preparation of Basalt Rock for Use in Corrosion Studies for the NRC Waste Packaging Program	Approved
WF-PP-34 Revision 0	Procedure for Preparation of Simulated Tuff Groundwater Solutions	To be Written

Table 5.1. Continued.

Procedure No.	Title	Status
WF-PP-35 Revision 1	Procedure for Performing Autoclave Exposures for Corrosion Tests in Simulated Brines	Approved
WF-PP-35.1 Revision 0	Procedure for Performing Autoclave Exposures for Corrosion Tests in Simulated Brines Using Sealed Internal Canister	Approved
WF-PP-36 Revision 0	Procedure for Performing Stagnant Autoclave Exposures for Corrosion Tests in Simulated Basalt or Tuff Groundwaters	Approved
WF-PP-37 Revision 0	Laboratory Procedure for Preparing Polarization Resistance Specimens, Performing Polarization Resistance Measurements and Evaluating Polarization Resistance Data	Approved
WF-PP-37.1 Revision 0	Laboratory Procedure for Performing Eh and Corrosion Potential Measurements in Autoclave Exposures in Simulated Basalt and Tuff Groundwater	Approved
WF-PP-37.2 Revision 0	Laboratory Procedure for Determination of the Polarization Behavior of Metal Specimens at Ambient Pressure	Approved
WF-PP-38 Revision 0	Procedure for Preparing and Evaluation of U-Bend Specimens for Stress Corrosion Studies of Overpack Materials for the NRC Waste Packaging Project	Approved
WF-PP-38.1 Revision 0	Procedure for Performing and Evaluating 3 Point Bend Beam Specimens for Stress Corrosion Studies of Overpack Materials for NRC Waste Package Program	Approved

Table 5.1. Continued.

Procedure No.	Title	Status
WF-PP-39 Revision 0	Procedure for Preparing, Testing and Evaluating Crevice Corrosion Specimens of Titanium Grade-12 and Cast Steel	Approved
WF-PP-40 Revision 0	Laboratory Procedures for Preparation, Cleaning, and Evaluation of Thermogalvanic and Heat-Transfer Specimens	Approved
WF-PP-41 Revision 0	Laboratory Procedures for Determination of Corrosion Rates Under Heat-Transfer Conditions	Approved
WF-PP-42 Revision 0	Laboratory Procedure for Determination of Thermogalvanic Corrosion Rates	Approved
WF-PP-43 Revision 0	Procedure for Welding Titanium Grade-12 Plate for Use in Corrosion Studies of Overpack Materials for NRC Waste Isolation Project	Approved
WF-PP-44 Revision 0	Procedure for Welding Cast and Wrought Steel Specimens	To be Written
WF-PP-45 Revision 0	Laboratory Procedure for Preparing and Evaluating Slow Strain-Rate Specimens and for Performing Slow Strain-Rate Tests	Approved
WF-PP-45.1 Revision 0	Laboratory Procedures for Performing Slow Strain-Rate Tests Under Potentiostated Conditions	Approved
WF-PP-46 Revision 0	Procedure for Preparation of Titanium Grade-12 Corrosion Specimens with Metallic Iron Embedded in the Surface	Approved

DISTRIBUTION LIST

Office of Regulatory Research
Division of Radiation Programs and Earth Sciences
Mail Stop 1130 SS
U.S. Nuclear Regulatory Commission, Washington, D.C. 20555

Attn: Division Director/Deputy Director
E. F. Conti, Chief, Waste Management Branch
F. A. Costanzi
J. R. Randall
M. B. McNeil
K. S. Kim, Project Manager

Division of Waste Management, NMSS
Mail Stop 623 SS
U.S. Nuclear Regulatory Commission, Washington, D.C. 20555

Attn: Division Director/Deupty Director
Chief, Engineering Branch
E. A. Wick
M. Tokar
K. C. Chang
Document Control Center

Advisory Committee on Reactor Safeguards
Mail Stop H-1016
U.S. Nuclear Regulatory Commission, Washington, D.C. 20555

Attn: Waste Management Subcommittee
R. C. Tang

Battelle's Columbus Laboratories
505 King Avenue
Columbus, Ohio 43201-2693

Attn: D. Stahl, Program Manager

DISTRIBUTION LIST (Continued)

Martin A. Molecke
Sandia National Lab.
Albuquerque, NM 87185

Neville Pugh
National Bureau of Standards
Washington, D.C. 20234

Nicholas Grant
Department of Metallurgy
Massachusetts Institute
of Technology
Cambridge, MA 02139

Jerome Kruger
Corrosion Section
National Bureau of Standards
Washington, D.C. 20234

Tae-Moon Ann
Brookhaven National Lab.
Upton, NY 11973

Don J. Bradley
Waste Package Programs
Battelle Pacific Northwest Labs
Richland, WA 99352

Allen G. Goff
Oak Ridge National Laboratory
P.O. Box X
Oak Ridge, TN 37830

Lynn Hobbs
Department of Materials Science
Massachusetts Institute of
Technology
77 Massachusetts Avenue
Cambridge, MA 02139

Richard E. Westerman
Pacific Northwest Lab.
P.O. Box 999
Richland, WA 99352

Thomas D. Chikalla
Pacific Northwest Lab.
P.O. Box 999
Richland, WA 99352

John Crandall
Savannah River Lab.
Aiken, SC 29808

Edward J. Hennelly
Savannah River Lab.
Aiken, SC 29808

Arthur A. Bauer
Office of Nuclear Waste Isolation
Battelle Memorial Institute
505 King Avenue
Columbus, OH 43201

Michael Smith
Basalt Waste Isolation Projects
Rockwell Hanford Operation
Richland, WA 99352

Kenneth Russell
Department of Materials Science
and Engineering
Massachusetts Institute of
Technology
Cambridge, MA 02139

Robert H. Doremus
Materials Engineering Department
Rensselaer Polytechnic Institute
Troy, NY 12181

David C. Kocher
Oak Ridge National Lab.
P.O. Box X
Oak Ridge, TN 37830

Stanley Wolf
DOE/BES
Washington, D.C. 20585

Neville Moody
Sandia Livermore Lab.
Livermore, CA 94550

Donald E. Clark
ONWI
Battelle Memorial Institute
505 King Avenue
Columbus, OH 43201

DISTRIBUTION LIST (Continued)

Martin Seitz
Argonne National Lab.
Argonne, IL 60439

Martin J. Steindler
Argonne National Lab.
Argonne, IL 60439

Donald G. Schweitzer
Brookhaven National Lab.
Upton, NY 11973

Peter Soo
Brookhaven National Lab.
Upton, NY 11973

David Martin
Iowa State University
Ames, IA 50011

Harold Wollenberg
Lawrence Berkeley Lab.
Berkeley, CA 94720

Nestor Ortiz
Sandia National Lab.
Albuquerque, NM 87185

Pedro B. Macedo
Catholic University of America
Washington, D.C. 20064

Robert Williams
Electric Power Research Institute
P.O. Box 10412
Palo Alto, CA 94301

William P. Reed
U.S. Department of Commerce
National Bureau of Standards
Washington, D.C. 20234

Ray Walton
U.S. Department of Energy
Washington, D.C. 20545

John E. Mendel
Materials Characterization Center
Pacific Northwest Lab.
Richland, WA 99352

Larry Hench
University of Florida
Gainesville, FL 32611

Davis E. Clark
University of Florida
Gainesville, FL 32611

Joseph Mascara
MS 5650 NL
U.S. Nuclear Reg. Comm.
Washington, DC 20555

Ken W. Stephens
The Aerospace Corp., Suite 400
955 L'Enfant Plaza, S.W.
Washington, DC 20024

Robert S. Dyer
Office of Radiation Programs (ANR-461)
U.S. Environmental Protection Agency
401 M Street, S.W.
Washington, DC 20460

Lorenzo Ricks
Office of Energy Research
U.S. Department of Energy
Washington, D.C. 20545

Larry Evans
Armco Research Center
703 Curtis Avenue
Middletown, OH 45043

Robert Gaugh
Armco Research Center
703 Curtis Avenue
Middletown, OH 45043

M. John Plodinec
Savannah River Laboratory
Aiken, SC 29808

Dennis R. Floyd
Manufacturing Sciences Corp.
711 Walnut Street
Boulder, CO 80302

BEST COPY AVAILABLE

NRC FORM 335 (11-81)

U.S. NUCLEAR REGULATORY COMMISSION

BIBLIOGRAPHIC DATA SHEET

1. REPORT NUMBER (Assigned by DDC)
NUREG/CR-3900, Vol. 3

4. TITLE AND SUBTITLE (Add Volume No., if appropriate)
Long-Term Performance of Materials Used for High-Level Waste Packaging: Quarterly Report, October-December 1984

2. (Leave blank)

3. RECIPIENT'S ACCESSION NO.

7. AUTHOR(S)
Compiled by D. Stahl and N. E. Miller

5. DATE REPORT COMPLETED
MONTH: March YEAR: 1985

9. PERFORMING ORGANIZATION NAME AND MAILING ADDRESS (Include Zip Code)
Battelle's Columbus Laboratories
505 King Avenue
Columbus, Ohio 43201-2693

DATE REPORT ISSUED
MONTH: May YEAR: 1985

6. (Leave blank)

8. (Leave blank)

12. SPONSORING ORGANIZATION NAME AND MAILING ADDRESS (Include Zip Code)
Division of Radiation Programs and Earth Sciences
Office of Nuclear Regulatory Research
U.S. Nuclear Regulatory Commission
Washington, D.C. 20555

10. PROJECT/TASK/WORK UNIT NO.

11. FIN NO.
B6764

13. TYPE OF REPORT
Quarterly

PERIOD COVERED (Inclusive dates)
October-December 1984

15. SUPPLEMENTARY NOTES

14. (Leave blank)

16. ABSTRACT (200 words or less)

Experiments for evaluating the glass-dissolution model are underway, and the procedure developed last quarter for dispersing RuO_2 in MCC 76-68 glass has been tested and proved to produce appropriate particle concentrations. Acetic and humic acids have been chosen to test the effect of natural organic acids on waste glass performance. In the overpack-corrosion effort, potentiodynamic polarization tests indicate that of the 15 chemical species tested, all but perchlorate and hydrogen may affect stress-corrosion cracking behavior of carbon steel; several synergistic effects were also indicated. In slow strain rate studies, specimens tested in 0.0005 M $FeCl_3$ (a much lower chloride concentration than expected in groundwater) exhibited significant cracking over the temperature range 250-315 C. Pits were found to propagate readily, but slowly, in 1018 carbon steel exposed to aerated basalt groundwater at 90 C. The general-corrosion correlation was changed to incorporate a finite rate of film growth. Integral experiments are being prepared to provide information on combined-effects processes that may influence the long-term performance of the waste package.

17. KEY WORDS AND DOCUMENT ANALYSIS

17a. DESCRIPTORS

High-level waste
Waste package
Waste form/container/overpack

17b. IDENTIFIERS/OPEN-ENDED TERMS

18. AVAILABILITY STATEMENT
Unlimited

19. SECURITY CLASS (This report)
Unclassified

21. NO. OF PAGES

20. SECURITY CLASS (This page)
Unclassified

22. PRICE
$

NRC FORM 335 (11-81)

*U.S. GOVERNMENT PRINTING OFFICE: 1985-461-721:20121

BEST COPY AVAILABLE